International Journal of Earth Sciences (2020) 109:2049–2079
https://doi.org/10.1007/s00531-020-01888-8

ORIGINAL PAPER

Dating of detrital zircons and tracing the provenance of quartzites from the Bystrzyckie Mts: implications for the tectonic setting of the Early Palaeozoic sedimentary basin developed on the Gondwana margin

Jacek Szczepański[1] · Krzysztof Turniak[1] · Robert Anczkiewicz[2] · Paulina Gleichner[1]

Received: 17 July 2019 / Accepted: 30 May 2020 / Published online: 9 June 2020

Abstract
We studied the petrographical characteristics and bulk chemical composition along with the age of detrital zircon grains from quartzites exposed in the western part of the Orlica-Śnieżnik dome in the Saxothuringian zone. Age spectra of detrital zircons were obtained by U–Pb laser ablation inductively coupled plasma mass spectrometry dating. The zircon ages define a few clusters of which the most numerous are Cambro-Ordovician and Neoproterozoic, and less frequent are Paleoproterozoic and Archean. A distinctive feature of the investigated samples is the lack of Mesoproterozoic zircon grains. The youngest age cluster documented in the investigated quartzites points to a Late Cambrian maximum depositional age and detritus derivation from erosion of Cambro-Ordovician metagranitoids. Bulk chemical composition of the quartzites indicates that they originated owing to erosion of granite within sedimentary basins developed on a passive continental margin. Presented data prove the similarity of the examined rocks to quartzites known from the eastern part of the Orlica-Śnieżnik dome and quartz metasandstones documented in other parts of the Variscan Belt of Europe known as the Armorican quartzites or their equivalents exposed in the Saxothuringian zone. Our results support the suggestion that the Orlica-Śnieżnik dome has an affinity to the West African Craton of the Gondwana margin and represents a fragment of the Saxothuringian zone.

Keywords Detrital zircon · Laser ablation ICP-MS · Saxothuringian zone · Orlica-Śnieżnik dome · Bohemian Massif

Introduction

The Variscan Belt of Europe comprises several terranes bearing a record of Neoproterozoic supra-subduction magmatic arc activity (Fig. 1). These terranes are commonly interpreted as derived from a long chain of Neoproterozoic continental magmatic arcs that developed along the Gondwana margin and are known as the Avalonian-Cadomian belt. The crustal fragments comprised within the belt are referred to in the literature as Cadomian and Avalonian terranes as well as Meguma, Ganderia, Carolina and Suwanee (e.g. Nance et al. 1991; van Staal et al. 1996; Pollock et al. 2012; Willner et al. 2014). Cadomian terranes are represented by e.g. the Armorican Massif, most of the Iberian Massif, Moldanubian and Saxothuringian zones of the Bohemian Massif (e.g. Murphy and Nance 1989; Fernández-Suárez et al. 2002a, b; Nance et al. 2002; Keppie et al. 2003; Linnemann et al. 2008), while Avalonian terranes comprise e.g., West and East Avalonia and Brunovistulicum of the Bohemian Massif (e.g. Finger et al. 2000; Friedl et al. 2004; Linnemann and Romer 2002; Fernandez-Suarez et al. 2003; Murphy et al. 2006; Drost et al. 2007). Subsequently, the Avalonian part of the belt was detached during Late Cambrian-Early Ordovician times from Gondwana during the formation of the Rheic Ocean (e.g. Linnemann et al. 2008; Murphy et al. 2009; Nance et al. 2010). This event was accompanied by the intrusion of several Cambro-Ordovician granites that intruded the crystalline basement of the Cadomian terranes (e.g. Kröner et al. 2001; von Raumer et al. 2002;

✉ Jacek Szczepański
jacek.szczepanski@uwr.edu.pl

[1] Institute of Geological Sciences, Faculty of Earth Science and Environmental Management, University of Wrocław, Pl. Maksa Borna 9, 50-205 Wrocław, Poland

[2] Institute of Geological Sciences, Polish Academy of Sciences, Research Centre in Cracow, Senacka 1, 31-002 Kraków, Poland

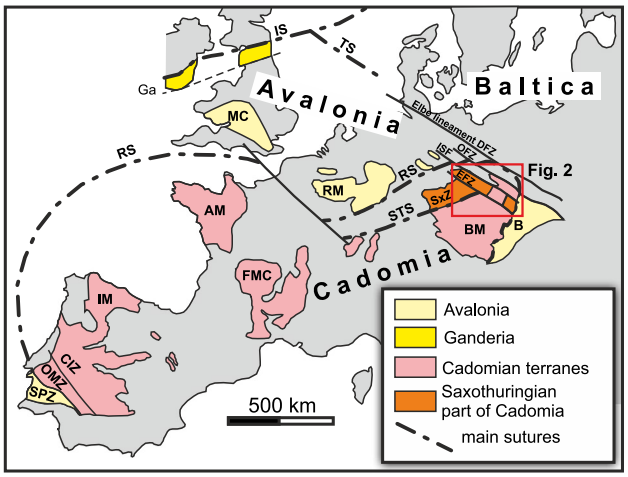

Fig. 1 Peri-Gondwanan terranes of southern and central Europe (modified from Franke 1989; Linnemann et al. 2007; Nance et al. 2008). *AM* Armorican Massif, *IM* Iberian Massif, *FMC* French Massif Central, BM Bohemian Massif, *RM* Rhenish Massif, *MC* Midland Craton, *B* Brunovistulicum, *SPZ* South Portuguese Zone, *OMZ* Ossa-Morena Zone, *CIZ* Central Iberian Zone, *SxZ* Saxothuringian Zone, *EFZ* Elbe Fault Zone, *ISF* Intra Sudetic Fault, *DFZ* Dolsk Fault Zone, *OFZ* Odra Fault Zone, *IS* Iapetus Suture, *RS* Rheic Suture, *STS* Saxothuringian Suture, *TS* Thor Suture

Košler et al. 2004; Martínez Catalán et al. 2009; Zieger et al. 2017). Described rifting occurred during the deposition of a quartz-rich, mature and relatively thick sedimentary sequence recognized in Central and Western Europe. The sequence is extending over entire NE-Africa and is known as the Armorican quartzite exposed in the Armorican and Iberian Massifs or time-equivalent quartzite horizons cropping out in the Saxothuringian zone (e.g. Linnemann et al. 2007; Linnemann et al. 2008; Domeier 2016). Consequently, the Gondwana margin contains a record of the transition from an arc to a rift followed by a passive margin tectonic setting (e.g. Linnemann et al. 2007).

One of the crustal domains in the Variscan Belt of Europe with preserved Cadomian and post-Cadomian volcano-sedimentary sequences is represented by the Saxothuringian zone (e.g. Linnemann et al. 2000; Buschmann et al. 2001; Žáčková et al. 2010). Its easternmost part extends into the West Sudetes where it is cut by the Teplá-Barrandian/Saxothuringian suture considered as the easternmost termination of the Saxothuringian zone (Fig. 2; Mazur and Aleksandrowski 2001). However, structural and geophysical data suggest that southeast of the Teplá-Barrandian/Saxothuringian suture the Saxothuringian crust is concealed below the Teplá-Barrandian domain (e.g. Chopin et al. 2012; Jeřábek et al. 2016). Furthermore, Chopin et al. (2012) and Mazur

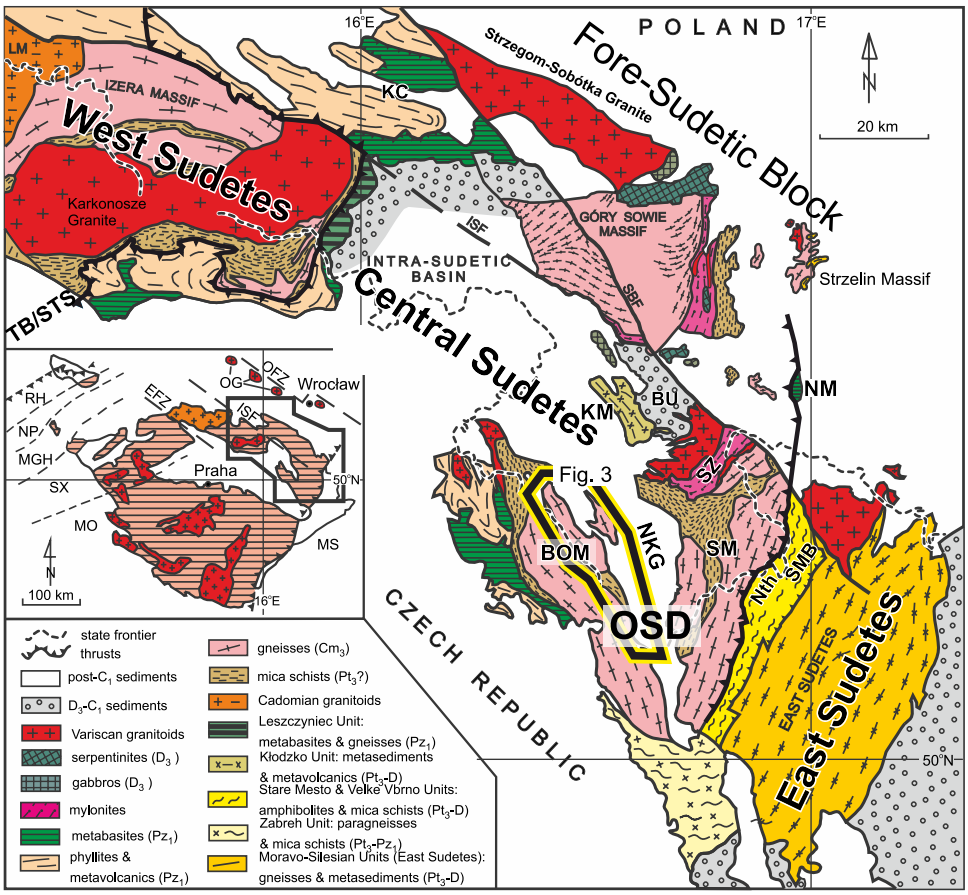

Fig. 2 Geological sketch map of the Sudetes after Mazur et al. (2006). *BU* Bardo Sedimentary unit, *BOM* Bystrzyca-Orlica Massif, *ISF* Intra-Sudetic fault, *KM* Kłodzko massif, *LM* Lusatian massif, *NKG* Nysa Kłodzka Graben, *NM* Niedźwiedź massif, *OSD* Orlica–Śnieżnik dome, *SBF* Sudetic boundary fault, *SM* Śnieżnik massif, *SMB* Staré Město Belt, *TB/STS* Teplá-Barrandian/Saxothuringian suture. Inset: *EFZ* Elbe Fault Zone, *MGH* Mid-German Crystalline High, *MO* Moldanubian zone, *MS* Moravo-Silesian zone, *NP* Northern Phyllite zone, *OG* Odra granitoids, *OFZ* Odra Fault Zone, *RH* Rhenohercynian zone, *SX* Saxothuringian zone. Age assignments: *Pt* Proterozoic, *Pz* Palaeozoic, *Cm* Cambrian, *Or* Ordovician, *D* Devonian, *C* Carboniferous; 1, Early; 2, Middle

et al. (2012) demonstrated that rock complexes of the Saxothuringian affinity emerge from below the Teplá-Barrandian domain in the Orlica-Śnieżnik dome (Central Sudetes). This view is supported by documentation of Neoproterozoic arc-derived volcano-sedimentary rock successions as well as Cambro-Ordovician passive margin sequence exposed in the Orlica-Śnieżnik dome (Mazur et al. 2012, 2015; Szczepański and Ilnicki 2014).

In this contribution, we present new data from whole-rock geochemistry and age spectra of detrital zircon populations derived from quartzite samples collected in the western part of the Orlica-Śnieżnik dome (the Bystrzyckie Mts) representing an allochtonous fragment of the Saxothuringian zone. The youngest obtained age cluster of the metamorphosed quartzitic sandstones is interpreted in terms of the maximum depositional age of the sedimentary protolith. Moreover, age spectra obtained from the whole analysed population of grains as well as bulk rock geochemistry were used to describe a possible provenance of the detrital material and tectonic setting of a depositional basin. The new data allowed to discuss a potential paleogeographic scenario leading to the formation of the examined quartzites and processes responsible for the deposition of the Cambro-Ordovician sedimentary cover on the Saxothuringian crust.

Geological setting

The Orlica-Śnieżnik dome in the Central Sudetes comprises medium-grade supracrustal successions of Neoproterozoic to Late Cambrian age surrounding Cambrian granite bodies later transformed into orthogneisses (Fig. 2). The dome is cut by the Upper Cretaceous Nysa Kłodzka Graben, which divides it into the eastern Śnieżnik massif and the western Bystrzyca-Orlica massif. However, despite several lithological similarities between both massifs division of the dome by the graben impede easy correlations of rock successions between the Bystrzyca-Orlica massif and the Śnieżnik massif.

Supracrustal successions exposed in the eastern part of the Orlica-Śnieżnik dome in the Śnieżnik massif are traditionally divided into: (1) the Młynowiec monotonous Formation composed of paragneisses intercalated with scarce basic metavolcanic rocks, (2) the Stronie variegated Formation dominated by micaschists interleaved with abundant bimodal volcanics and (3) a thin horizon of the Goszów quartzite (Fig. 3a, Don et al. 1990). The youngest detrital zircon population indicates a maximum sedimentation age of 563 ± 6 Ma, 532 ± 6 Ma and 490 ± 9 Ma for the Młynowiec Formation, the Stronie Formation and the Goszów quartzite, respectively. Hence they represent three distinct volcano-sedimentary successions (Mazur et al. 2012; Mazur et al. 2015; but see the alternative interpretation by Jastrzębski et al. 2010). The Neoproterozoic and Early Cambrian volcano-sedimentary successions in the Orlica-Śnieżnik dome were intruded by Mid- to Late Cambrian calc-alkaline granitoids with geochemical characteristics typical for crustal melts (Turniak et al. 2000). U–Pb mean ages, obtained by various methods, of magmatic zircons derived from orthogneiss range from 517 to 490 Ma and are interpreted as the time of intrusions (e.g. Turniak et al. 2000; Kröner et al. 2001; Lange et al. 2002).

Supracrustal successions in the western part of the Orlica-Śnieżnik dome (the Bystrzyca-Orlica massif) are not well recognized. The only age data comes from the Wyszki paragneiss (Fig. 3b) which comprises the monotonous metagreywacke succession with detrital zircon age spectra and maximum depositional age of 569 ± 8 Ma resembling metasedimentary rocks of the Młynowiec Formation exposed in the eastern part of the Orlica–Śnieżnik dome (Mazur et al. 2015). There are no data regarding maximum sedimentation age of the variegated succession dominated by mica schists from the western part of the Orlica-Śnieżnik dome (the Bystrzyca-Orlica massif). However, owing to the similar lithological inventory of this variegated succession and the Stronie Formation exposed in the Śnieżnik massif they are considered as equivalents. There are no age data for quartzite cropping out in the Bystrzyca-Orlica massif.

A lithostratigraphic scheme for the Neoproterozoic and Early Palaeozoic sequences exposed in the Orlica-Śnieżnik dome (Fig. 3a) was proposed by Szczepański and Ilnicki (2014). It shows similarities to other parts of the Variscan Belt of Europe e.g., the Saxothuringian zone in Germany as well as the entire Iberian Massif except for the South Portuguese zone (e.g. Bandres et al. 2002; Linnemann et al. 2007; Nance et al. 2008; Vintaned et al. 2009). In all mentioned areas extending west of the Central Sudetes well-preserved fragments of Cadomian basement and post-Cadomian cover with magmatic arc signature are covered by Late Cambrian–Early Ordovician quartz-rich metasandstones (e.g. Pereira et al. 2006; Linnemann et al. 2008). Similar quartzite is also known from the eastern part of the Orlica-Śnieżnik dome (the Śnieżnik massif) as the Goszów quartzite. This rock displays a Late Cambrian maximum deposition age (490 ± 9 Ma, Mazur et al. 2012) and chemical composition typical for sediments deposited on a passive continental margin (Szczepański and Ilnicki 2014). On the other hand, the youngest detrital zircons reported by Jastrzębski et al. (2010) for the Goszów quartzite yielded ages in the time interval of 460–470 Ma. Interestingly, in the Goszów quartzite, Jastrzębski et al. (2016) documented a population of monazite grains dated at 494 Ma believed to represent a significant admixture of volcanic material. Consequently, the latter authors suggested a metavolcanic origin for at least

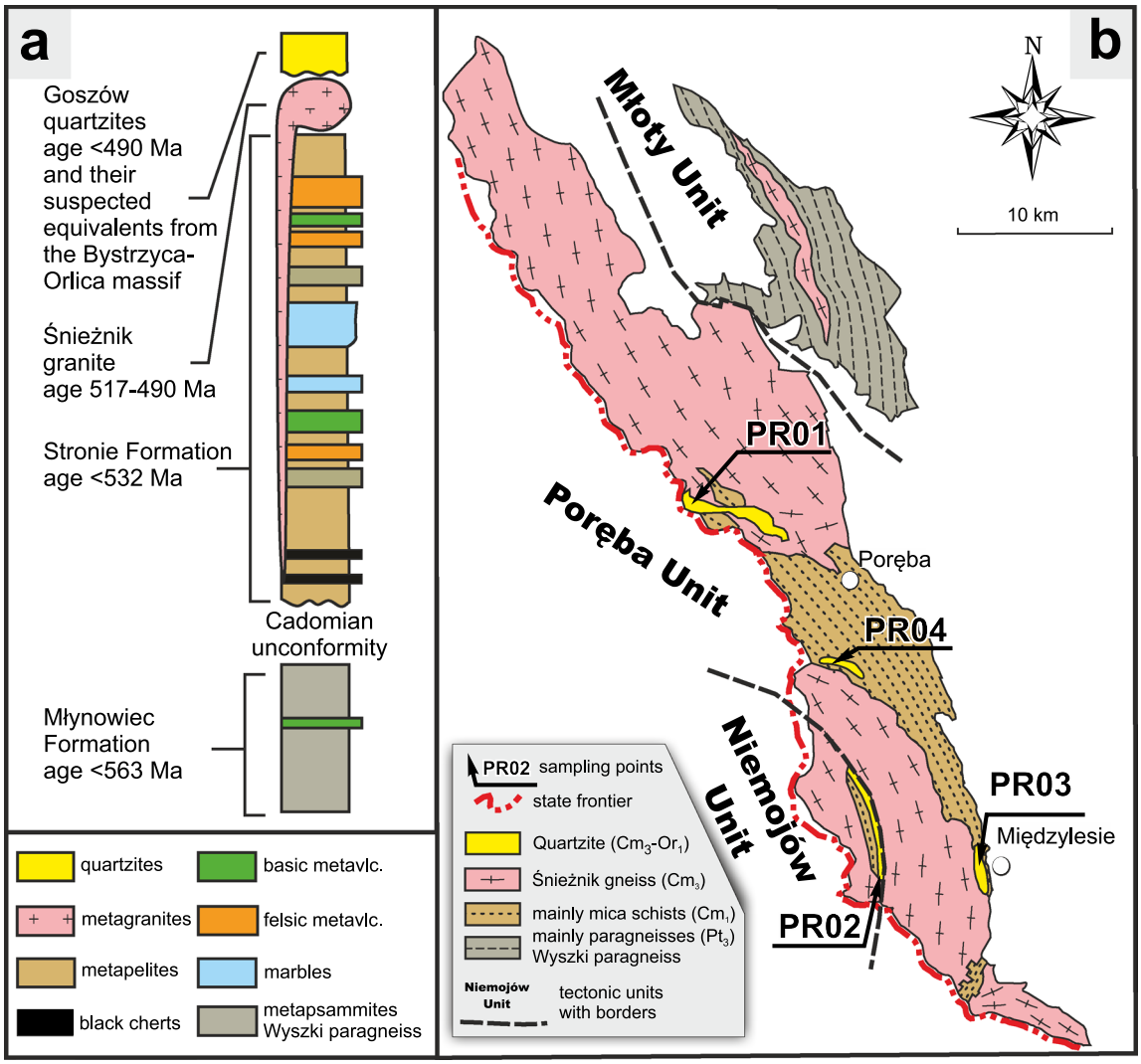

Fig. 3 **a** Generalized lithostratigraphic profile of volcano-sedimentary successions exposed in the Orlica-Śnieżnik dome (modified from Szczepański and Ilnicki 2014), **b** the Geological sketch map of the Bystrzyckie Mts. after (Szczepański 2010). PR01—E16°51′75.53″, N50°24′56.36″, PR02—E16°60′03.15″, N50°16′58.33″, PR03—E16°63′86.88″, N50°14′82.22″, PR04—E16°57′49.68″, N50°20′32.96″. GPS coordinates are given in WGS84 system

some of the quartzites cropping out in the eastern part of the Orlica-Śnieżnik dome (the Śnieżnik massif).

The Goszów quartzite, exposed in the eastern part of the Orlica-Śnieżnik dome (the Śnieżnik massif), form thin, continuous and relatively well-defined lithological horizon. On the other hand, quartzites are known from the western part of the dome crop out in various tectonic units of the Bystrzyckie Mts. representing Polish part of the Bystrzyca-Orlica massif and form small and isolated lenses aligned parallel to the foliation observed in surrounding supracrustal variegated succession and orthogneisses (Fig. 3b). Accordingly, the tectonic position of the quartzites in the western part of the dome (the Bystrzyckie Mts) is not similar to what is observed in the eastern part of the dome in the Śnieżnik massif. Therefore, despite lithological similarities between the Goszów quartzite and the quartzites known from the Bystrzyckie Mts. there is still uncertainty whether these rocks are equivalent or should rather be concerned as representing different lithostratigraphic members.

Sample description

Four quartzite samples were collected at four localities within different tectonic units of the Bystrzyckie Mts (Fig. 3b). Samples PR01, PR03 and PR04 come from the Poręba Unit, while sample PR02 was collected in the Niemojów Unit. Tectonic units identified in the Bystrzyckie Mts. were interpreted as fragments of the Variscan imbricated nappe stack (Szczepański 2010; Szczepański and Ilnicki

2014). In this part of the Bystrzyckie Mts. metamorphic gradient changes from biotite (sample PR01) to staurolite zone (samples PR02, PR03 and PR04) which is associated with the increase of temperature of metamorphism from c. 460 to 620 °C (Szczepański 2010).

The investigated quartzite samples range in colour from light to dark grey and represent fine- to medium-grained rocks composed mainly of quartz with secondary white mica. The latter mineral is particularly abundant in sample PR01 and to a lesser degree also in sample PR04. Major accessory minerals are represented by zircon, rutile, monazite, zoisite, tourmaline and opaques, which are especially abundant in samples PR01 and PR04. The foliation of these rocks is defined by parallel alignment of isolated white mica flakes or thin laminae composed exclusively of white micas.

Analytical methods

The bulk rock chemical analyses of quartzite samples were performed at Acme Analytical Laboratories Ltd. (Vancouver, Canada) and are summarized in Table 1. Major- and trace-element abundances were determined using ICP-MS following lithium metaborate fusion and nitric acid digestion of 0.2 g representative whole-rock powder. Loss on ignition (LOI) was measured by weight difference after ignition at 1000 °C and was found to be negligible for all samples (Table 1). Detection limits are within 0.01% for major elements, between 0.1–0.5 ppm for most trace elements, 1 ppm for Ba, Sn and Zn, and 8 ppm for V. Geochemical diagram from Fig. 4 was designed using the GCDKit software of Janoušek et al. (2006). Geochemical diagrams from Fig. 8 were designed via the R software environment (R Core Team 2012).

Mineral separation was carried out at the University of Wrocław following conventional techniques involving crushing, sieving, heavy liquids and Frantz magnetic separator. Zircon grains were hand-picked under a binocular so that representative population was achieved. Additionally, from sample PR01 we extracted one extra population represented only by the euhedral crystals. Subsequently, the zircons were mounted in an epoxy resin and polished. Cathodoluminescent images of zircons were conducted using a Philips XL30 electron microscope (15 kV and 1 nA) at the Faculty of Earth Sciences, University of Silesia, Sosnowiec, Poland.

In situ U–Pb zircon dating by laser ablation inductively coupled plasma mass spectrometry (LA ICP-MS) was conducted at the Kraków Research Centre, Institute of Geological Sciences, Polish Academy of Sciences. The analyses were carried out using an excimer laser (ArF) RESOlution M-50 by Resonetics (now Applied Spectra) coupled with an ICP-MS XseriesII by ThermoFisher Scientific. Detailed description of the apparatus and the applied analytical

Table 1 The major and trace element composition of the studied quartzites from the Bystrzyckie Mts.

Sample	PR01	PR02	PR03	PR04
SiO_2	86.29	95.58	95.91	93.21
Al_2O_3	8.06	1.74	2.02	3.91
Fe_2O_3	0.94	1.18	0.64	0.94
MgO	0.19	0.03	0.07	0.08
CaO	0.02	0.02	0.01	0.07
Na_2O	0.04	0.03	0.02	0.07
K_2O	2.67	0.55	0.62	0.60
TiO_2	0.19	0.03	0.03	0.11
$P2O_5$	0.02	0.01	0.02	0.05
MnO	0.01	0.01	0.01	0.01
Cr_2O_3	0.00	0.00	0.00	0.00
LOI	1.50	0.80	0.60	0.80
Total	99.93	100.01	99.99	99.97
Ba	425	31	63	801
Rb	154.6	29.4	39.5	49.2
Ga	9.5	1.9	2	5
Sr	19.4	17.2	96.3	26.8
Ni	1	2.1	0.7	1.4
Nb	4.3	1.1	0.7	2.8
Hf	4.1	0.7	0.9	5
Zr	150.4	20.9	29.6	202.4
Y	18.1	0.8	1.3	7.5
Th	7.6	1	1.2	3.5
Ta	0.5	0.05	0.05	0.3
U	1.6	0.7	1.7	1.4
Sc	4	0.5	0.5	2
Co	0.7	1	0.5	1
V	16	4	4	4
Cs	6.8	1.3	2.4	5.8
Pb	4.2	3	1.9	4.5
Sn	4	0.5	0.5	4
La	18	4	3	5.6
Ce	35.3	7.4	5.8	11.5
Pr	4.11	0.7	0.67	1.21
Nd	15.8	2.8	2.8	4.5
Sm	3.21	0.32	0.68	0.96
Eu	0.43	0.08	0.14	0.23
Gd	2.96	0.3	0.51	0.95
Tb	0.51	0.03	0.05	0.18
Dy	3.23	0.15	0.27	1.16
Ho	0.72	0.02	0.04	0.24
Er	2.13	0.09	0.14	0.79
Tm	0.3	0.005	0.02	0.11
Yb	2.04	0.12	0.21	0.88
Lu	0.31	0.01	0.03	0.14

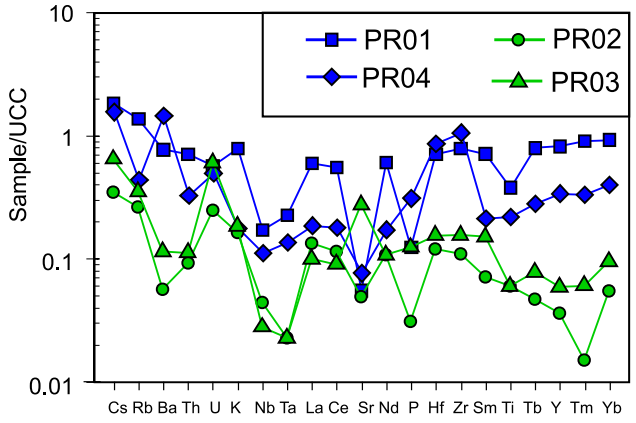

Fig. 4 Upper continental crust (UCC)-normalized major-element pattern for Orlica-Śnieżnik dome metasediments. Normalization factors after Taylor and McLennan (1995)

conditions are presented in Anczkiewicz and Anczkiewicz (2016). Zircon Z91500 (Wiedenbeck et al. 1995) was used as a primary standard and zircons GJ-1 (Jackson et al. 2004) and Plešovice (Sláma et al. 2008) were frequently measured for the quality control. Each eight unknowns or secondary standards, two primary standards were measured. We applied 30 µm laser spot size, with 5 Hz repetition rate and fluence of about 3 J/cm^2. For each analytical session, the secondary standards yielded $^{206}Pb/^{238}U$ mean ages accurate within about 1% precision (2 relative standard deviations) which is satisfactory for the purpose of the provenance studies.

From each sample at least 100 zircon crystals were dated. Analyses with more than 10% discordance (% discordance = [1 − ($^{206}Pb/^{238}U$ age)/($^{207}Pb/^{235}U$ age)] × 100%) were rejected. Concordia plots were prepared using the Isoplot/Ex 4.15 (Ludwig 2008). Frequency as well as kernel density plots were designed via the R software environment (R Core Team 2012). For zircons older than 1 Ga $^{207}Pb/^{206}Pb$ ages were taken for interpretation and the $^{206}Pb/^{238}U$ ages were utilised for the younger grains.

Results

Major and trace elements characteristics

The studied quartzite samples show significant differences in geochemical composition. Samples PR01 and PR04 show lower SiO_2 content (ranging from 86.3 to 93.2 wt%), relatively high Al_2O_3 (in the range between 3.9 and 8.06 wt%) and generally display a higher abundance of trace elements in comparison to samples PR02 and PR03 (Table 1; Fig. 4). Chemical variability correlates with the abundance of white mica and accessory minerals including zircon, rutile, monazite tourmaline and epidote group minerals. When normalized to the composition of the upper continental crust, the studied quartzites show rather variable patterns but all display a clear negative Nb and Ta anomaly (Fig. 4), which very likely is a feature inherited from felsic crustal material bearing supra-subduction affinity (e.g. Baier et al. 2008; Gonçalves et al. 2016). It is also worth to point out that relatively high Zr and Hf concentration compared to the upper continental crust is especially well visible in the case of sample PR04.

The studied metasediments underwent greenschist to amphibolite facies metamorphism that could have mobilised the large-ion lithophile elements (e.g., Na, K). However, any large-scale remobilization of REEs, Th, Zr, Sc, Cr and Co seems unlikely. Furthermore, the latter elements are considered as transferred quantitatively into clastic sediments during weathering and transportation, thus reflecting the signature of the parent materials (Bhatia and Crook 1986; McLennan 1989).

Morphology and zonation description of analysed zircons

Sample PR01

The zircon population of sample PR01 ranges from 75 to 350 µm with the mean length of 160 µm. They are dominated by grains with elongation less than 2 (73%), whereas zircons with elongation in the range of 2–3 are less frequent (27%). Inspected zircon grains are often ovoid (40%) to well-rounded (36%), while euhedral crystals form quite an important group (24%). Most grains are transparent and pinkish (60%). Yellow and brown grains are rare (13%), while 27% of the analysed zircons display orange, yellow or brown patches. Some grains have small and unrecognised mineral inclusions. Most of the grains in the investigated sample are homogenous, while 17% of them display inherited cores. Analysed zircons can be grouped into two classes characterized by: (1) well-developed prism {110} and {211} ditetragonal bipyramids as well as (2) prism {100} and bipyramid {101}. All studied grains, including euhedral crystals, show clear signs of mechanical reworking with strongly rounded shapes. In case of euhedral crystals, it is typified by slightly rounded prisms and bipyramid faces and uneven crystal surfaces (Fig. 5a).

Sample PR02

The PR02 sample is dominated by rounded to well-rounded grains (91%) and subhedral to euhedral crystals constitute a relatively small group (9%). Their length varies from 75 to 425 µm with a mean length of 182 µm and elongation mostly below 2. Zircons from this sample are transparent,

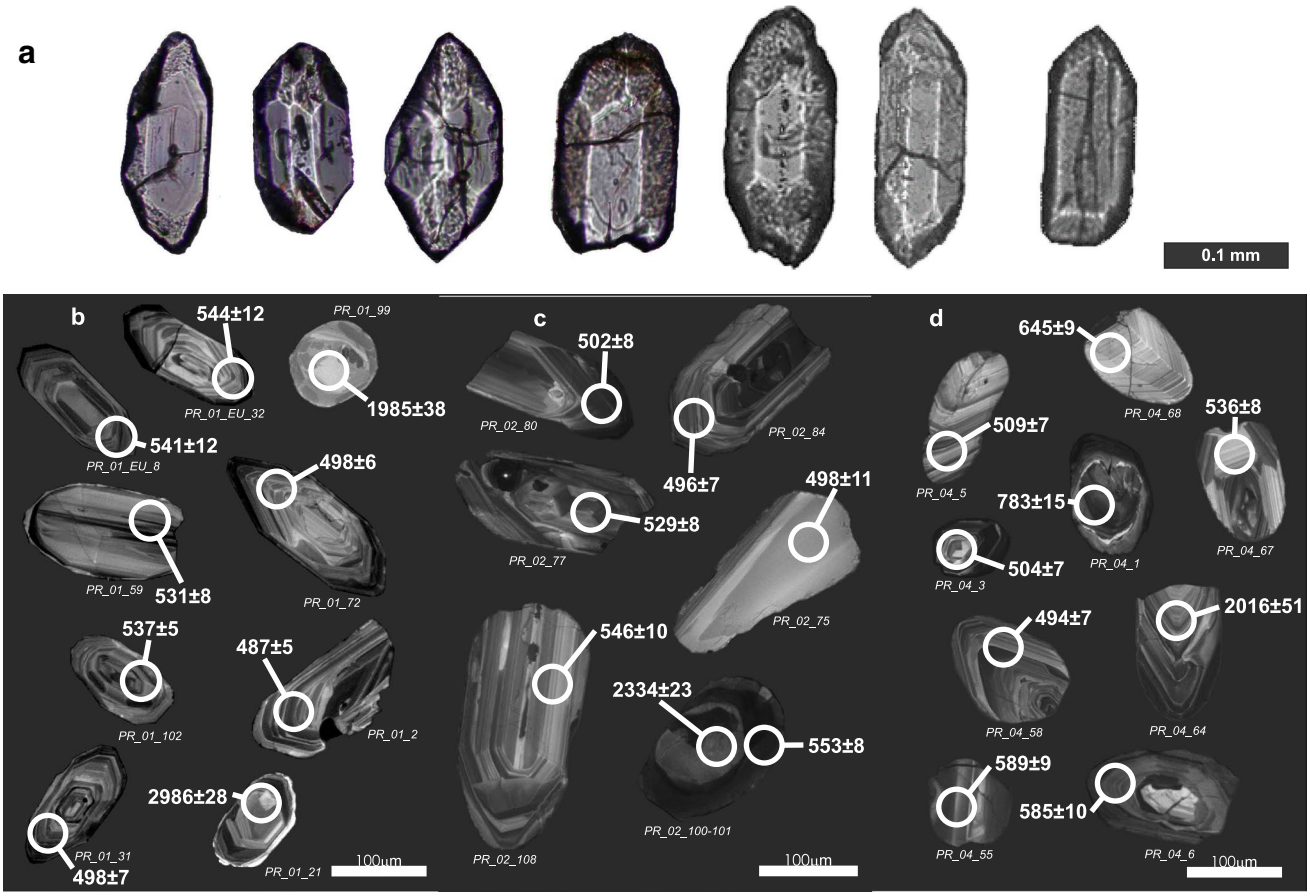

Fig. 5 **a** Transmitted light images of zircons. Examples of cathodo-luminescence images of zircon grains from: **b** sample PR01, **c** PR02 and **d** PR04. Grain numbers and ages (Ma) refer to Tables 2, 3, 4 and 5; uncertainties are 1σ

colourless (24%) to yellowish-brown (49%). 27% of grains are translucent with the cloudy interior. Commonly the analysed zircons have mineral inclusions. Majority of the grains are homogenous, while 19% of them display inherited cores. Euhedral crystals form two major groups: (1) with {100} prisms and ditetragonal bipyramid {211} equally well developed and (2) with {100} prisms dominating over bipyramids {101}. Euhedral crystals in this sample are characterized by slightly rounded bipyramid terminations.

Sample PR03

Zircons in sample PR03 range in length from 85 to 260 µm with the mean length of 150 µm and elongation below 2. This sample is dominated by rounded to well-rounded grains (88% of the population), whereas euhedral crystals form a relatively small group (12% of population). 50% of zircons are colourless and transparent, 40% of grains is characterized by orange colour, while 10% of the population is translucent and brownish. Majority of grains is homogenous, whereas only a few zircons exhibit inherited cores. Subhedral and euhedral crystals define two groups: (1) with well-developed {110} prism and bipyramid {211} and (2) with well-developed {100} prism and bipyramid {101}. All investigated subhedral and euhedral crystals display traces of mechanical reworking typified by slightly rounded bipyramid terminations.

Sample PR04

Zircon grains in sample PR04 range in length from 75 to 275 µm with a mean length of 140 µm and elongation mostly below 2. The vast majority of grains constitute rounded and well-rounded grains (95% of the population). Euhedral and subhedral crystals (5% of the population) are characterized by slightly rounded bipyramid terminations as well as uneven and stained crystal surfaces. 52% of grains are colourless and transparent, whereas 39% of zircons display orange to red spots. Euhedral and subhedral crystals can be subdivided into two groups: (1) with well-developed {110} prism and bipyramid {211} as well as (2) {100} prism and bypiramid {101}. Importantly, even the group of euhedral

grains display slightly rounded bypiramid terminations and stained crystal faces (Fig. 5a).

CL images of inspected zircon populations reveal that all the investigated grains show similar characteristics in terms of brightness and internal textures. Majority of the grains display moderate cathodoluminescense and show fine oscillatory zoning of clearly magmatic origin (e.g. PR_01_72, Fig. 5b). The second group of grains is characterized by ovoid shape and complex internal texture most probably related to metamorphic growth (e.g. PR_01_59, Fig. 5b). Few grains from both groups contain xenocrystic cores (e.g. PR_02_100-101, Fig. 5c; PR_04_1 and PR_04_1, Fig. 5d) and sporadically display thin and dark rims (e.g. PR_02_80, Fig. 5c; PR_04_64, 5d).

Summing up, the vast majority of euhedral zircon grains strongly resemble those from the Cambro-Ordovician metagranites with respect to morphology and CL. They are widespread in the Orlica-Śnieżnik dome and are known as the Śnieżnik orthogneiss (e.g. Turniak et al. 2000). Moreover, all inspected grains, including euhedral crystals, show clear signs of mechanical reworking characterised by slightly rounded prisms and bipyramid faces as well as stained crystal faces (Fig. 5a). It is worth to note that in the studied zircon populations we have not identified any grains with morphology typical of volcanic rocks.

Laser ablation ICP-MS U–Pb zircon dating

The results of laser ablation ICP-MS U–Pb zircon dating of quartzites PR01, PR02 and PR04 are summarized in Tables 2, 3, 4 and 5 and Figs. 6 and 7. The frequency histograms were constructed using 25 Ma bin width and were presented jointly with the kernel density plots applying 15 Ma smoothing wavelength (Fig. 7).

All three samples show similar zircon age distribution patterns. Concordia plots show the largest number of zircons belonging to the Ordovician–Neoproterozoic time. Much smaller populations are displayed by the Paleoproterozoic zircons and only sporadically Archean zircons are present (Figs. 6, 7). Histograms allow a more detailed view and show that about 71–80% of the zircons represent the time span between ca. 0.48 and 0.88 Ga. The youngest crystals represent the Early Ordovician ages and constitute 3–9% of the whole population (Fig. 7). One of the two most prominent age probability peaks, clearly marked in all three samples, corresponds to ca. 0.50 Ga. The second noticeable peak at 0.58 Ga is present in samples PR01 and PR04. In sample PR01, this is the dominant age component. All histograms show an asymmetric tail from the Neoproterozoic and Cambrian maxima towards older ages with small probability peaks around 0.70 and 0.80 Ga. The Neoproterozoic and the Phanerozoic zircons are euhedral with only slight signs of mechanical abrasion, they are fairly dark in CL and commonly display oscillatory zoning (Fig. 5b–d). The remaining zircon defines small maxima throughout most of the Paleoproterozoic (with decreasing number of ages towards the Early Paleoproterozoic) and scarce in the Archean with the oldest crystals dated at 2.99 Ga. The Paleoproterozoic (15–23% of total analysed zircons) and the Archaean zircons (up to 6.5% of total analysed zircons) are commonly rounded, fractured and show variable zoning patterns (Fig. 5b–d). Notably, a common feature observed in all quartzites is the lack of Mesoproterozoic and Grenvillian (0.98–1.25 Ga) zircons. To more closely constrain the time of sedimentation, from sample PR01, we extracted, supposedly the youngest, euhedral crystals and analysed them separately (Fig. 7b, PR01EU). Zircons from this sample are strongly dominated by the Phanerozoic and the Neoproterozoic density peaks at 0.50 Ga and 0.55 Ga and contain only a few older Neoproterozoic (0.68, 0.77, 0.95 Ga) as well as Paleoproterozoic (1.77 and 1.90 Ga) grains (Fig. 7b). This demonstrates that the source for the detritus comprised in the inspected quartzites represents Cambrian and Neoproteorozoic metagranitoids.

Discussion

Provenance signature and tectonic setting of the sedimentary basin

Provenance of sedimentary rocks can be tested using La/Sc vs. Th/Co diagram proposed by Cullers (2002). Siliciclastic rocks derived from erosion of felsic rocks are enriched in elements incompatible in igneous melts including Th and La, whereas those derived from a mafic source are enriched in elements compatible in igneous melts including Sc and Co. Therefore, La/Sc and Th/Co ratios are useful in tracking the nature of the source area. For quartzite samples from the Bystrzyckie Mts. La/Sc and Th/Co ratios range from 2.5 to 8.0 and from 1.0 to 10.8, respectively, pointing to a source area dominated by felsic rocks (Fig. 8a). Conclusions concerning lithology of the source area are confirmed by inspection of the Th/Sc vs. Zr/Sc diagram devised by McLennan et al. (1993). These ratios increase towards more felsic members of a magmatic suite and the elements utilised in this diagram are characterized by low residence times in natural waters (Taylor and McLennan 1985). The investigated quartzites are located close to the line describing typical magmatic suite and display relatively high Th/Sc (1.75–2.40) and Zr/Sc (37.60–101.2) ratios typifying granites as a potential source for the detritus (Fig. 8b). Interestingly, sample PR04 departs from this pattern by its very high Zr/Sc ratio compared to the remaining samples (Fig. 8b). This is indicative of sedimentary sorting and recycling processes that presumably influenced chemical composition of

Table 2 Laser ablation ICP-MS U–Pb isotopic data of detrital zircons from sample PR01

Analysis	Isotopic ratios						Calculated ages Ma					
	$^{207}Pb/^{235}U$	±2 sigma	$^{206}Pb/^{238}U$	±2 sigma	$^{207}Pb/^{206}Pb$	±2 sigma	$^{207}Pb/^{235}U$	±2 sigma	$^{206}Pb/^{238}U$	±2 sigma	$^{207}Pb/^{206}Pb$	±2 sigma
Z PR01-13-1-3_1	7.1800	0.1600	0.3888	0.0038	0.1340	0.0026	2129	20	2116	18	2138	34
Z PR01-13-1-4_1	11.3100	0.2400	0.4705	0.0053	0.1738	0.0033	2549	19	2485	23	2588	32
Z PR01-13-1-12	6.0500	0.1800	0.3438	0.0050	0.1283	0.0038	1974	27	1903	24	2044	55
Z PR01-13-1-16	5.2600	0.1400	0.3223	0.0040	0.1187	0.0028	1857	23	1800	20	1922	41
Z PR01-13-1-24	4.9820	0.1000	0.3189	0.0029	0.1132	0.0020	1813	18	1784	14	1844	32
Z PR01-13-1-25	0.9180	0.0400	0.1038	0.0014	0.0648	0.0028	654	21	636	8	659	91
Z PR01-13-1-29	0.7720	0.0300	0.0923	0.0011	0.0611	0.0024	577	18	569	7	556	84
Z PR01-13-1-32	1.2850	0.0600	0.1346	0.0021	0.0695	0.0032	827	27	814	12	803	95
Z PR01-13-1-37	5.3800	0.1300	0.3263	0.0036	0.1201	0.0028	1877	21	1819	18	1938	41
Z PR01-13-1-38	10.1400	0.2100	0.4548	0.0042	0.1617	0.0028	2445	19	2416	19	2466	30
Z PR01-13-1-45	0.8140	0.0460	0.0923	0.0018	0.0649	0.0039	594	27	570	10	610	130
Z PR01-13-1-52	0.7020	0.0200	0.0834	0.0009	0.0611	0.0016	538	12	516	5	602	56
Z PR01-13-1-56	6.5700	0.1600	0.3701	0.0039	0.1283	0.0026	2048	21	2029	18	2066	35
Z PR01-13-1-57	0.6650	0.0420	0.0794	0.0017	0.0606	0.0039	515	25	493	10	570	140
Z PR01-13-1-63	27.1500	0.5800	0.7283	0.0085	0.2693	0.0047	3384	21	3524	32	3298	28
Z PR01-13-1-68	0.8180	0.0280	0.0948	0.0011	0.0625	0.0021	602	16	584	7	630	72
Z PR01-13-1-73	6.5950	0.1400	0.3669	0.0040	0.1300	0.0024	2057	19	2014	19	2098	32
Z PR01-13-1-76	10.5600	0.2600	0.4659	0.0057	0.1643	0.0038	2478	23	2464	25	2486	38
Z PR01-13-1-78	0.9950	0.0350	0.1087	0.0017	0.0662	0.0021	697	19	665	10	757	73
Z PR01-13-1-91	5.6170	0.1300	0.3222	0.0053	0.1262	0.0023	1915	21	1799	26	2037	32
Z PR01-13-1-94	1.4160	0.0440	0.1460	0.0017	0.0703	0.0021	889	19	878	10	894	63
Z PR01-13-1-95	5.5700	0.1800	0.3539	0.0050	0.1140	0.0036	1901	28	1951	24	1823	61
Z PR01-13-1-100	21.8800	0.5200	0.6457	0.0085	0.2453	0.0046	3172	23	3208	33	3148	30
Z PR01-13-1-106	21.0600	0.5200	0.5957	0.0095	0.2557	0.0040	3133	25	3007	39	3215	24
Z PR01-13-1-107	6.9840	0.1400	0.4022	0.0039	0.1255	0.0022	2108	19	2178	18	2029	33
Z PR01-13-1-109	7.0570	0.1300	0.3768	0.0032	0.1355	0.0021	2117	17	2061	15	2165	28
Z PR01-13-1-1	0.8030	0.0470	0.0963	0.0015	0.0611	0.0037	582	27	592	9	460	120
Z PR01-13-1-2	0.6140	0.0230	0.0784	0.0008	0.0569	0.0020	481	14	487	5	414	76
Z PR01-13-1-5	0.7800	0.0410	0.0943	0.0015	0.0601	0.0032	584	24	581	9	550	120
Z PR01-13-1-8	0.7630	0.0410	0.0952	0.0014	0.0585	0.0032	561	23	586	8	400	110
Z PR01-13-1-9	0.7820	0.0440	0.0945	0.0015	0.0598	0.0032	580	25	582	9	520	110
Z PR01-13-1-10	0.7410	0.0320	0.0914	0.0012	0.0587	0.0025	558	19	564	7	491	93
Z PR01-13-1-14	0.8040	0.0280	0.0960	0.0010	0.0606	0.0020	594	16	591	6	566	70
Z PR01-13-1-17	0.6840	0.0340	0.0852	0.0014	0.0578	0.0028	525	21	527	8	470	110

Table 2 (continued)

Analysis	Isotopic ratios						Calculated ages Ma					
	$^{207}Pb/^{235}U$	±2 sigma	$^{206}Pb/^{238}U$	±2 sigma	$^{207}Pb/^{206}Pb$	±2 sigma	$^{207}Pb/^{235}U$	±2 sigma	$^{206}Pb/^{238}U$	±2 sigma	$^{207}Pb/^{206}Pb$	±2 sigma
Z PR01-13-1-18	0.7850	0.0380	0.0936	0.0016	0.0606	0.0028	589	23	577	10	600	100
Z PR01-13-1-19	7.3700	0.1800	0.3992	0.0052	0.1332	0.0030	2156	21	2164	24	2141	39
Z PR01-13-1-20	0.6700	0.0260	0.0855	0.0010	0.0566	0.0021	517	16	529	6	429	79
Z PR01-13-1-21	18.1500	0.3800	0.5926	0.0063	0.2212	0.0038	2996	20	2999	25	2986	28
Z PR01-13-1-22	0.7650	0.0300	0.0950	0.0011	0.0584	0.0022	570	17	585	6	464	80
Z PR01-13-1-23	0.6830	0.0350	0.0849	0.0013	0.0583	0.0029	524	21	525	8	470	110
Z PR01-13-1-27	0.8370	0.0520	0.0969	0.0019	0.0631	0.0040	609	29	596	11	600	140
Z PR01-13-1-28	0.8860	0.0260	0.1061	0.0011	0.0608	0.0017	641	15	650	6	585	62
Z PR01-13-1-29	0.7700	0.0300	0.0924	0.0011	0.0609	0.0024	576	18	570	7	549	84
Z PR01-13-1-31	0.6430	0.0390	0.0804	0.0012	0.0576	0.0035	501	24	498	7	470	130
Z PR01-13-1-33	0.7370	0.0210	0.0915	0.0009	0.0584	0.0015	558	12	564	5	508	57
Z PR01-13-1-34	0.6340	0.0260	0.0803	0.0010	0.0573	0.0023	492	17	498	6	428	85
Z PR01-13-1-36	0.8440	0.0320	0.1002	0.0013	0.0616	0.0023	616	18	615	8	585	80
Z PR01-13-1-39	0.8680	0.0320	0.1041	0.0011	0.0603	0.0021	627	17	638	7	551	75
Z PR01-13-1-42	0.8490	0.0800	0.0984	0.0024	0.0631	0.0059	591	43	605	14	420	190
Z PR01-13-1-43	0.8630	0.0760	0.1006	0.0025	0.0631	0.0056	594	42	617	14	400	180
Z PR01-13-1-44	0.8270	0.0520	0.0961	0.0015	0.0626	0.0041	596	30	591	9	520	130
Z PR01-13-1-46	0.8730	0.0710	0.1053	0.0022	0.0602	0.0049	599	40	645	13	350	160
Z PR01-13-1-47	0.7520	0.0350	0.0923	0.0012	0.0592	0.0028	559	20	569	7	470	99
Z PR01-13-1-50	0.7810	0.0380	0.0957	0.0015	0.0596	0.0029	576	22	590	9	463	100
Z PR01-13-1-51	0.7960	0.0360	0.0956	0.0012	0.0602	0.0027	584	20	589	7	500	93
Z PR01-13-1-53	0.8760	0.0610	0.1039	0.0019	0.0613	0.0042	612	34	637	11	430	140
Z PR01-13-1-54	0.7520	0.0280	0.0927	0.0010	0.0585	0.0021	563	16	571	6	486	79
Z PR01-13-1-58	7.6200	0.2400	0.4009	0.0052	0.1375	0.0041	2174	28	2171	24	2169	53
Z PR01-13-1-59	0.6650	0.0310	0.0858	0.0013	0.0562	0.0027	515	19	531	8	410	110
Z PR01-13-1-60	0.7730	0.0340	0.0936	0.0012	0.0603	0.0027	572	19	577	7	506	94
Z PR01-13-1-61	0.6090	0.0400	0.0788	0.0014	0.0563	0.0037	466	25	489	9	290	130
Z PR01-13-1-62	0.8520	0.0290	0.1016	0.0012	0.0611	0.0019	624	16	623	7	591	71
Z PR01-13-1-64	0.6800	0.0290	0.0863	0.0010	0.0567	0.0024	521	18	534	6	404	91
Z PR01-13-1-65	0.8250	0.0440	0.0980	0.0016	0.0618	0.0034	597	25	603	9	500	110
Z PR01-13-1-66	0.7470	0.0250	0.0929	0.0010	0.0583	0.0019	564	15	572	6	497	71
Z PR01-13-1-67	0.8250	0.0430	0.1012	0.0015	0.0590	0.0030	596	24	621	9	440	110
Z PR01-13-1-69	0.7090	0.0470	0.0850	0.0014	0.0604	0.0040	534	27	526	9	490	140
Z PR01-13-1-70	0.8860	0.0310	0.1063	0.0012	0.0605	0.0020	641	17	651	7	562	72
Z PR01-13-1-71	0.8060	0.0430	0.0975	0.0015	0.0598	0.0032	587	25	600	9	460	110

Table 2 (continued)

Analysis	Isotopic ratios						Calculated ages Ma					
	$^{207}Pb/^{235}U$	±2 sigma	$^{206}Pb/^{238}U$	±2 sigma	$^{207}Pb/^{206}Pb$	±2 sigma	$^{207}Pb/^{235}U$	±2 sigma	$^{206}Pb/^{238}U$	±2 sigma	$^{207}Pb/^{206}Pb$	±2 sigma
Z PR01-13-1-72	0.6370	0.0270	0.0803	0.0010	0.0576	0.0025	493	17	498	6	417	91
Z PR01-13-1-74	7.6900	0.1700	0.4039	0.0039	0.1378	0.0027	2192	20	2186	18	2190	36
Z PR01-13-1-75	1.1600	0.0420	0.1281	0.0015	0.0657	0.0024	777	21	777	9	733	82
Z PR01-13-1-79	0.9130	0.0370	0.1090	0.0015	0.0609	0.0024	653	19	667	8	564	81
Z PR01-13-1-80	0.6910	0.0270	0.0854	0.0010	0.0586	0.0022	527	16	528	6	472	81
Z PR01-13-1-81	0.8780	0.0530	0.1017	0.0017	0.0630	0.0039	637	30	624	10	610	130
Z PR01-13-1-83	0.9030	0.0380	0.1091	0.0014	0.0597	0.0023	643	20	667	8	506	85
Z PR01-13-1-85	0.7640	0.0320	0.0939	0.0012	0.0591	0.0024	568	18	579	7	479	84
Z PR01-13-1-88	0.7380	0.0430	0.0920	0.0015	0.0585	0.0034	545	25	567	9	400	120
Z PR01-13-1-89	0.9720	0.0390	0.1133	0.0015	0.0623	0.0025	683	20	691	9	619	83
Z PR01-13-1-90	6.8000	0.1800	0.3822	0.0044	0.1292	0.0033	2079	25	2085	21	2066	46
Z PR01-13-1-92	0.6140	0.0240	0.0786	0.0010	0.0565	0.0022	480	15	488	6	398	82
Z PR01-13-1-93	6.6800	0.2100	0.3754	0.0056	0.1277	0.0039	2061	27	2053	26	2056	54
Z PR01-13-1-97	1.0120	0.0420	0.1169	0.0016	0.0632	0.0027	699	22	713	10	608	92
Z PR01-13-1-98	7.0900	0.3000	0.3865	0.0072	0.1328	0.0055	2112	36	2105	33	2103	72
Z PR01-13-1-99	6.2400	0.1500	0.3677	0.0039	0.1231	0.0027	2007	20	2018	18	1985	38
Z PR01-13-1-101	0.6290	0.0320	0.0799	0.0011	0.0571	0.0029	487	20	496	7	390	110
Z PR01-13-1-102	0.6970	0.0250	0.0869	0.0009	0.0580	0.0020	533	15	537	5	473	73
Z PR01-13-1-104	0.8040	0.0400	0.0954	0.0014	0.0617	0.0031	590	23	587	9	530	110
Z PR01-13-1-105	0.6870	0.0240	0.0866	0.0010	0.0576	0.0020	526	14	536	6	445	75
Z PR01-13-1-108	0.7500	0.0290	0.0932	0.0012	0.0586	0.0023	561	17	574	7	468	86
Z PR01-13-1-110	6.8900	0.1700	0.3826	0.0043	0.1301	0.0030	2094	23	2088	20	2088	42
Z PR01-13-1-111	0.6240	0.0260	0.0785	0.0010	0.0578	0.0024	488	17	487	6	437	88

Table 3 Laser ablation ICP-MS U–Pb isotopic data of detrital zircons from sample PR01EU

Analysis	Isotopic ratios						Calculated ages Ma					
	$^{207}Pb/^{235}U$	±2 sigma	$^{206}Pb/^{238}U$	±2 sigma	$^{207}Pb/^{206}Pb$	±2 sigma	$^{207}Pb/^{235}U$	±2 sigma	$^{206}Pb/^{238}U$	±2 sigma	$^{207}Pb/^{206}Pb$	±2 sigma
Z PR-01-13EU-4	1.9160	0.0950	0.1792	0.0044	0.0767	0.0035	1064	34	1062	24	986	100
Z PR-01-13EU-2	0.8700	0.0810	0.0968	0.0035	0.0634	0.0055	628	45	595	20	700	170
Z PR-01-13EU-6	0.6210	0.0260	0.0800	0.0018	0.0562	0.0021	487	17	496	11	405	82
Z PR-01-13EU-7	0.6900	0.0360	0.0882	0.0020	0.0568	0.0027	526	21	545	12	395	100
Z PR-01-13EU-18	0.6880	0.0290	0.0803	0.0018	0.0621	0.0023	528	17	498	11	616	81
Z PR-01-13EU-24	0.7510	0.0420	0.0884	0.0022	0.0620	0.0033	560	25	546	13	560	110
Z PR-01-13EU-27	1.1950	0.0480	0.1257	0.0029	0.0684	0.0023	790	22	763	17	828	70
Z PR-01-13EU-29	5.8800	0.2200	0.3612	0.0084	0.1184	0.0037	1951	33	1986	40	1899	57
Z PR-01-13EU-34	4.6520	0.1400	0.3051	0.0067	0.1104	0.0027	1754	26	1716	33	1791	44
Z PR-01-13EU-35	0.5850	0.0350	0.0810	0.0020	0.0530	0.0031	466	24	502	12	260	120
Z PR-01-13EU-71	0.8160	0.0450	0.0912	0.0022	0.0655	0.0035	599	25	562	13	690	110
Z PR-01-13EU-72	0.7880	0.0370	0.0864	0.0020	0.0662	0.0029	582	21	534	12	715	94
Z PR-01-13EU-74	0.8260	0.0300	0.0953	0.0021	0.0627	0.0019	608	17	587	13	649	67
Z PR-01-13EU-75	0.5660	0.0340	0.0783	0.0021	0.0529	0.0031	456	22	486	12	270	120
Z PR-01-13EU-79	0.6930	0.0300	0.0880	0.0021	0.0573	0.0023	531	18	544	12	448	88
Z PR-01-13EU-92	0.6760	0.0360	0.0827	0.0019	0.0595	0.0030	519	22	512	11	500	110
Z PR-01-13EU-94	0.6030	0.0230	0.0794	0.0018	0.0548	0.0018	477	15	493	11	360	72
Z PR-01-13EU-1	0.7440	0.0430	0.0892	0.0022	0.0609	0.0034	559	26	551	13	540	120
Z PR-01-13EU-3	0.8660	0.0350	0.1010	0.0023	0.0622	0.0023	628	19	620	13	605	79
Z PR-01-13EU-5	0.7870	0.0370	0.0947	0.0022	0.0601	0.0026	581	21	583	13	511	88
Z PR-01-13EU-8	0.7160	0.0310	0.0876	0.0020	0.0592	0.0023	546	18	541	12	519	82
Z PR-01-13EU-9	0.7900	0.0340	0.0930	0.0023	0.0614	0.0024	590	20	573	13	617	89
Z PR-01-13EU-10	0.6950	0.0310	0.0857	0.0020	0.0588	0.0023	531	18	530	12	484	86
Z PR-01-13EU-11	0.7750	0.0390	0.0930	0.0022	0.0605	0.0029	573	22	573	13	504	100
Z PR-01-13EU-12	0.7470	0.0410	0.0933	0.0023	0.0587	0.0031	555	24	575	14	430	110
Z PR-01-13EU-13	0.8140	0.0410	0.0953	0.0023	0.0620	0.0030	597	23	587	14	562	100
Z PR-01-13EU-14	1.1780	0.0880	0.1262	0.0035	0.0681	0.0050	766	42	766	20	680	150
Z PR-01-13EU-15	0.8070	0.0440	0.0966	0.0023	0.0607	0.0031	594	25	594	14	550	110
Z PR-01-13EU-16	0.6670	0.0300	0.0826	0.0018	0.0583	0.0024	515	18	512	11	470	85
Z PR-01-13EU-17	0.7490	0.0700	0.0911	0.0029	0.0603	0.0056	529	40	563	17	280	170
Z PR-01-13EU-19	0.6320	0.0320	0.0827	0.0020	0.0556	0.0026	493	20	512	12	356	98
Z PR-01-13EU-20	0.7430	0.0360	0.0916	0.0022	0.0588	0.0026	559	21	565	13	473	95
Z PR-01-13EU-21	0.6530	0.0320	0.0812	0.0019	0.0584	0.0026	506	19	503	11	452	93
Z PR-01-13EU-22	0.8700	0.0360	0.1008	0.0023	0.0625	0.0023	630	20	619	14	617	82

Table 3 (continued)

Analysis	Isotopic ratios						Calculated ages Ma					
	$^{207}Pb/^{235}U$	±2 sigma	$^{206}Pb/^{238}U$	±2 sigma	$^{207}Pb/^{206}Pb$	±2 sigma	$^{207}Pb/^{235}U$	±2 sigma	$^{206}Pb/^{238}U$	±2 sigma	$^{207}Pb/^{206}Pb$	±2 sigma
Z PR-01-13EU-23	0.8020	0.0410	0.0950	0.0023	0.0613	0.0030	593	23	585	13	550	100
Z PR-01-13EU-25	0.7940	0.0320	0.0953	0.0022	0.0601	0.0021	590	18	586	13	566	76
Z PR-01-13EU-26	0.6640	0.0320	0.0779	0.0019	0.0617	0.0028	513	20	483	12	605	100
Z PR-01-13EU-28	0.7640	0.0340	0.0933	0.0022	0.0593	0.0024	570	20	575	13	494	86
Z PR-01-13EU-30	5.5600	0.3400	0.3413	0.0110	0.1195	0.0072	1856	55	1886	52	1760	120
Z PR-01-13EU-31	0.6120	0.0300	0.0772	0.0018	0.0578	0.0026	480	19	480	10	421	92
Z PR-01-13EU-32	0.7240	0.0340	0.0883	0.0020	0.0590	0.0025	547	19	546	12	488	87
Z PR-01-13EU-33	0.8210	0.0290	0.0985	0.0022	0.0603	0.0019	606	17	606	13	570	68
Z PR-01-13EU-36	0.6950	0.0300	0.0865	0.0020	0.0585	0.0023	532	18	535	12	491	85
Z PR-01-13EU-37	0.6650	0.0340	0.0839	0.0020	0.0571	0.0026	512	21	519	12	439	100
Z PR-01-13EU-38	0.7110	0.0380	0.0865	0.0021	0.0597	0.0030	542	22	535	12	500	110
Z PR-01-13EU-39	0.6390	0.0280	0.0812	0.0019	0.0575	0.0023	500	17	503	11	470	90
Z PR-01-13EU-41	0.7590	0.0350	0.0937	0.0022	0.0586	0.0025	567	21	577	13	465	92
Z PR-01-13EU-42	0.7060	0.0340	0.0887	0.0021	0.0577	0.0025	536	20	548	12	434	95
Z PR-01-13EU-43	0.7480	0.0490	0.0898	0.0024	0.0608	0.0039	547	29	555	14	430	130
Z PR-01-13EU-47	0.8290	0.0520	0.0994	0.0027	0.0608	0.0037	599	30	612	16	460	130
Z PR-01-13EU-48	0.7620	0.0480	0.0910	0.0023	0.0606	0.0037	560	28	561	14	470	130
Z PR-01-13EU-49	0.7610	0.0380	0.0912	0.0022	0.0607	0.0029	569	22	562	13	542	99
Z PR-01-13EU-51	0.8760	0.0450	0.1012	0.0026	0.0628	0.0029	633	24	622	15	629	100
Z PR-01-13EU-52	0.6980	0.0280	0.0870	0.0020	0.0581	0.0021	533	17	538	12	469	79
Z PR-01-13EU-53	0.6120	0.0250	0.0789	0.0019	0.0560	0.0020	481	16	489	11	407	77
Z PR-01-13EU-54	0.6480	0.0300	0.0806	0.0019	0.0583	0.0025	501	18	500	11	450	90
Z PR-01-13EU-56	0.8850	0.0650	0.1018	0.0030	0.0638	0.0046	629	35	625	17	550	150
Z PR-01-13EU-57	0.7030	0.0280	0.0880	0.0020	0.0581	0.0020	538	17	543	12	488	75
Z PR-01-13EU-58	0.7590	0.0390	0.0924	0.0022	0.0595	0.0029	565	22	570	13	476	100
Z PR-01-13EU-60	1.5710	0.0600	0.1581	0.0036	0.0720	0.0024	954	24	946	20	948	70
Z PR-01-13EU-61	0.9610	0.0430	0.1113	0.0026	0.0626	0.0025	677	23	680	15	609	88
Z PR-01-13EU-62	0.6720	0.0340	0.0847	0.0020	0.0571	0.0026	515	21	524	12	405	98
Z PR-01-13EU-63	0.7140	0.0310	0.0891	0.0020	0.0581	0.0024	542	19	550	12	455	89
Z PR-01-13EU-65	0.7160	0.0360	0.0875	0.0022	0.0591	0.0027	544	21	540	13	524	100
Z PR-01-13EU-66	0.6230	0.0250	0.0790	0.0018	0.0569	0.0020	488	16	490	11	437	73
Z PR-01-13EU-67	0.6250	0.0300	0.0786	0.0018	0.0572	0.0025	486	19	488	11	423	95
Z PR-01-13EU-68	0.6490	0.0280	0.0806	0.0019	0.0584	0.0023	505	17	500	11	475	84
Z PR-01-13EU-70	0.6830	0.0310	0.0851	0.0020	0.0585	0.0025	526	19	527	12	488	94
Z PR-01-13EU-76	0.6230	0.0240	0.0794	0.0018	0.0565	0.0018	489	15	493	10	430	70

Table 3 (continued)

Analysis	Isotopic ratios						Calculated ages Ma					
	$^{207}Pb/^{235}U$	±2 sigma	$^{206}Pb/^{238}U$	±2 sigma	$^{207}Pb/^{206}Pb$	±2 sigma	$^{207}Pb/^{235}U$	±2 sigma	$^{206}Pb/^{238}U$	±2 sigma	$^{207}Pb/^{206}Pb$	±2 sigma
Z PR-01-13EU-77	0.7020	0.0310	0.0876	0.0020	0.0579	0.0023	537	18	541	12	486	89
Z PR-01-13EU-78	0.6790	0.0270	0.0849	0.0019	0.0579	0.0020	523	16	525	11	465	74
Z PR-01-13EU-80	0.6210	0.0280	0.0794	0.0018	0.0567	0.0024	485	17	492	11	395	87
Z PR-01-13EU-81	0.6500	0.0310	0.0797	0.0019	0.0593	0.0026	504	19	494	11	503	92
Z PR-01-13EU-82	0.6310	0.0260	0.0799	0.0018	0.0568	0.0021	493	17	496	11	429	80
Z PR-01-13EU-85	0.8700	0.0680	0.1041	0.0029	0.0603	0.0045	610	36	638	17	410	150
Z PR-01-13EU-87	0.6880	0.0340	0.0875	0.0021	0.0567	0.0027	524	21	541	12	390	99
Z PR-01-13EU-88	0.7420	0.0430	0.0917	0.0022	0.0586	0.0031	549	25	565	13	420	110
Z PR-01-13EU-89	0.6950	0.0380	0.0870	0.0022	0.0582	0.0030	530	23	538	13	450	110
Z PR-01-13EU-90	0.6390	0.0280	0.0818	0.0019	0.0568	0.0023	500	18	507	11	418	85
Z PR-01-13EU-91	0.7010	0.0320	0.0876	0.0020	0.0578	0.0024	534	20	541	12	444	91
Z PR-01-13EU-95	0.7310	0.0430	0.0921	0.0023	0.0578	0.0034	548	26	568	14	390	120
Z PR-01-13EU-96	0.6870	0.0390	0.0880	0.0022	0.0569	0.0031	519	24	543	13	350	110
Z PR-01-13EU-97	0.6070	0.0300	0.0780	0.0018	0.0566	0.0027	477	19	484	11	381	98
Z PR-01-13EU-98	0.6420	0.0280	0.0804	0.0018	0.0578	0.0023	501	17	498	11	466	84
Z PR-01-13EU-99	0.7260	0.0460	0.0909	0.0023	0.0577	0.0034	545	27	561	14	430	130
Z PR-01-13EU-101	0.8650	0.0530	0.1007	0.0025	0.0623	0.0035	621	29	618	15	560	120

Table 4 Laser ablation ICP-MS U–Pb isotopic data of detrital zircons from sample PR02

Analysis	Isotopic ratios						Calculated ages Ma					
	$^{207}Pb/^{235}U$	±2 sigma	$^{206}Pb/^{238}U$	±2 sigma	$^{207}Pb/^{206}Pb$	±2 sigma	$^{207}Pb/^{235}U$	±2 sigma	$^{206}Pb/^{238}U$	±2 sigma	$^{207}Pb/^{206}Pb$	±2 sigma
PR02-1	6.6250	0.0840	0.3740	0.0044	0.1278	0.0016	2060	11	2048	21	2061	22
PR02-2	0.6330	0.0140	0.0806	0.0010	0.0569	0.0013	497	8	500	6	459	51
PR02-4	0.6170	0.0250	0.0809	0.0012	0.0553	0.0023	487	16	501	7	382	92
PR02-5	0.7440	0.0320	0.0935	0.0015	0.0577	0.0025	558	19	576	9	434	93
PR02-6	1.0250	0.0400	0.1151	0.0018	0.0641	0.0025	710	20	702	11	691	86
PR02-7	0.8870	0.0430	0.1016	0.0017	0.0632	0.0031	639	23	624	10	650	100
PR02-8	0.6250	0.0320	0.0792	0.0014	0.0571	0.0029	489	20	491	8	430	110
PR02-9	6.2800	0.1900	0.3716	0.0073	0.1228	0.0040	2011	27	2043	37	1982	60
PR02-11	0.6280	0.0250	0.0804	0.0012	0.0563	0.0023	489	16	499	7	390	86
PR02-12	0.6310	0.0300	0.0796	0.0013	0.0575	0.0028	488	19	494	8	400	100
PR02-13	7.2700	0.4200	0.4010	0.0100	0.1313	0.0068	2132	52	2173	46	2087	92
PR02-14	7.5000	0.1900	0.4002	0.0062	0.1354	0.0034	2163	23	2168	29	2144	46
PR02-15	4.9700	0.1300	0.3136	0.0048	0.1146	0.0030	1807	22	1757	24	1850	48
PR02-16	0.6100	0.0160	0.0781	0.0010	0.0565	0.0016	481	10	485	6	427	63
PR02-18	0.8570	0.0420	0.0994	0.0017	0.0630	0.0032	621	23	611	10	590	110
PR02-19	12.0300	0.2500	0.4909	0.0077	0.1772	0.0035	2603	20	2578	35	2619	33
PR02-20	0.6310	0.0270	0.0800	0.0013	0.0571	0.0025	494	17	496	8	424	91
PR02-21	0.7410	0.0260	0.0931	0.0014	0.0575	0.0020	559	15	574	8	453	76
PR02-22	1.1320	0.0520	0.1151	0.0023	0.0717	0.0036	763	25	702	13	910	110
PR02-23	0.8570	0.0300	0.1004	0.0015	0.0621	0.0023	627	17	617	9	626	82
PR02-24	0.6470	0.0120	0.0828	0.0010	0.0565	0.0011	505	8	513	6	451	43
PR02-26	0.6690	0.0210	0.0843	0.0012	0.0575	0.0018	516	13	522	7	463	68
PR02-27	0.8450	0.0250	0.1013	0.0013	0.0606	0.0019	617	14	622	8	562	67
PR02-28	0.6080	0.0190	0.0778	0.0011	0.0567	0.0018	479	12	483	7	425	71
PR02-29	19.5700	0.6400	0.5810	0.0140	0.2458	0.0083	3066	32	2949	56	3148	54
PR02-32	5.4900	0.3300	0.3437	0.0088	0.1148	0.0068	1844	52	1903	43	1710	120
PR02-33	0.6870	0.0210	0.0866	0.0013	0.0572	0.0017	529	13	535	8	472	67
PR02-34	0.6140	0.0190	0.0788	0.0011	0.0565	0.0018	484	12	489	7	432	69
PR02-35	6.4500	0.1000	0.3657	0.0050	0.1279	0.0021	2041	13	2009	24	2068	28
PR02-36	0.8520	0.0280	0.1005	0.0014	0.0614	0.0021	626	15	617	8	616	75
PR02-37	0.8210	0.0300	0.1019	0.0015	0.0585	0.0022	604	17	625	9	471	83
PR02-38	0.6410	0.0240	0.0820	0.0011	0.0565	0.0021	501	15	509	7	448	80
PR02-39	0.5970	0.0490	0.0805	0.0018	0.0542	0.0047	471	31	499	11	310	180
PR02-40	15.4800	0.4400	0.5590	0.0120	0.2011	0.0059	2836	28	2858	48	2816	47

Table 4 (continued)

Analysis	Isotopic ratios						Calculated ages Ma					
	$^{207}Pb/^{235}U$	±2 sigma	$^{206}Pb/^{238}U$	±2 sigma	$^{207}Pb/^{206}Pb$	±2 sigma	$^{207}Pb/^{235}U$	±2 sigma	$^{206}Pb/^{238}U$	±2 sigma	$^{207}Pb/^{206}Pb$	±2 sigma
PR02-41	0.6290	0.0320	0.0827	0.0014	0.0554	0.0026	492	20	512	8	380	100
PR02-42	6.7400	0.1300	0.3653	0.0056	0.1339	0.0028	2072	18	2006	26	2141	35
PR02-43	0.7180	0.0270	0.0897	0.0014	0.0583	0.0022	545	16	554	8	461	81
PR02-44	0.6610	0.0250	0.0824	0.0012	0.0579	0.0022	510	15	511	7	451	80
PR02-45	0.6020	0.0370	0.0796	0.0016	0.0553	0.0036	474	24	494	10	350	140
PR02-46	0.7620	0.0270	0.0952	0.0013	0.0580	0.0022	572	15	586	8	475	83
PR02-48	0.6190	0.0180	0.0790	0.0010	0.0568	0.0017	486	11	490	6	437	65
PR02-49	0.7780	0.0300	0.0922	0.0013	0.0610	0.0024	583	17	569	8	581	86
PR02-50	0.6150	0.0130	0.0775	0.0010	0.0575	0.0012	485	8	481	6	479	47
PR02-53	0.6230	0.0210	0.0812	0.0011	0.0556	0.0019	488	13	503	7	378	75
PR02-55	0.8880	0.0520	0.1024	0.0019	0.0616	0.0037	636	28	630	11	600	120
PR02-56	0.6640	0.0470	0.0824	0.0018	0.0586	0.0041	497	29	510	11	350	140
PR02-57	4.9400	0.2100	0.3240	0.0063	0.1109	0.0052	1805	34	1809	30	1768	88
PR02-58	0.7790	0.0450	0.0914	0.0019	0.0625	0.0037	574	26	564	11	520	130
PR02-59	0.6860	0.0180	0.0875	0.0011	0.0569	0.0015	528	11	541	7	445	56
PR02-60	0.6190	0.0210	0.0797	0.0011	0.0565	0.0020	488	13	494	7	419	73
PR02-62	0.6640	0.0310	0.0849	0.0013	0.0569	0.0027	509	19	525	8	383	99
PR02-63	0.6000	0.0230	0.0782	0.0012	0.0556	0.0023	475	15	486	7	400	94
PR02-64	0.6280	0.0240	0.0794	0.0012	0.0571	0.0022	491	15	493	7	440	81
PR02-65	0.7920	0.0340	0.0949	0.0015	0.0607	0.0028	588	20	585	9	542	96
PR02-66	0.7120	0.0300	0.0894	0.0013	0.0577	0.0025	541	18	552	8	439	93
PR02-68	0.6410	0.0340	0.0794	0.0013	0.0586	0.0032	492	22	492	8	420	120
PR02-70	0.6110	0.0230	0.0782	0.0012	0.0567	0.0022	481	15	486	7	413	82
PR02-72	0.6630	0.0390	0.0843	0.0016	0.0574	0.0035	514	24	522	10	400	130
PR02-73	0.6280	0.0270	0.0803	0.0017	0.0571	0.0026	493	17	498	10	450	100
PR02-74	0.8660	0.0430	0.1063	0.0018	0.0591	0.0030	620	24	651	10	440	110
PR02-75	0.6440	0.0520	0.0804	0.0019	0.0592	0.0051	483	33	498	11	310	160
PR02-77	0.6830	0.0340	0.0856	0.0014	0.0579	0.0030	523	21	529	8	450	110
PR02-78	0.6590	0.0170	0.0822	0.0011	0.0583	0.0016	511	10	509	7	493	60
PR02-80	0.6360	0.0290	0.0810	0.0014	0.0569	0.0027	496	19	502	8	420	100
PR02-82	5.4100	0.1000	0.3292	0.0052	0.1190	0.0020	1883	17	1834	25	1933	31
PR02-83	5.7600	0.1500	0.3464	0.0059	0.1208	0.0028	1938	21	1917	28	1961	40
PR02-84	0.6410	0.0250	0.0801	0.0012	0.0582	0.0024	497	16	496	7	446	87
PR02-87	0.6320	0.0260	0.0799	0.0014	0.0575	0.0026	495	16	496	8	455	96
PR02-88	0.6640	0.0240	0.0829	0.0013	0.0577	0.0021	513	15	513	8	465	80

Table 4 (continued)

Analysis	Isotopic ratios						Calculated ages Ma					
	$^{207}Pb/^{235}U$	±2 sigma	$^{206}Pb/^{238}U$	±2 sigma	$^{207}Pb/^{206}Pb$	±2 sigma	$^{207}Pb/^{235}U$	±2 sigma	$^{206}Pb/^{238}U$	±2 sigma	$^{207}Pb/^{206}Pb$	±2 sigma
PR02-89	0.7560	0.0610	0.0976	0.0025	0.0559	0.0046	562	34	600	15	370	170
PR02-90	0.7120	0.0310	0.0859	0.0014	0.0601	0.0027	540	18	531	8	500	96
PR02-91	0.6340	0.0200	0.0806	0.0012	0.0571	0.0019	496	13	500	7	439	73
PR02-93	0.7090	0.0340	0.0888	0.0016	0.0585	0.0030	541	21	549	9	460	110
PR02-94	0.7960	0.0220	0.0955	0.0013	0.0603	0.0016	592	12	588	8	574	58
PR02-95	0.7070	0.0260	0.0871	0.0012	0.0586	0.0021	537	16	538	7	485	81
PR02-96	4.3120	0.0920	0.3007	0.0041	0.1041	0.0024	1688	18	1694	20	1669	42
PR02-97	0.6850	0.0230	0.0864	0.0012	0.0575	0.0020	525	14	534	7	449	74
PR02-98	6.7300	0.1200	0.3834	0.0051	0.1272	0.0022	2073	15	2092	24	2046	31
PR02-99	0.6410	0.0300	0.0816	0.0014	0.0571	0.0029	500	19	505	9	430	110
PR02-100	7.9300	0.1200	0.3814	0.0067	0.1494	0.0020	2220	14	2081	31	2334	23
PR02-101	0.7350	0.0260	0.0895	0.0013	0.0594	0.0021	556	15	553	8	521	77
PR02-102	0.7220	0.0350	0.0906	0.0016	0.0580	0.0029	544	21	560	10	430	100
PR02-103	11.4400	0.1500	0.4687	0.0060	0.1766	0.0022	2558	12	2477	27	2617	21
PR02-104	0.7020	0.0290	0.0884	0.0014	0.0579	0.0025	535	18	546	8	440	90
PR02-105	0.6120	0.0320	0.0801	0.0014	0.0558	0.0030	486	21	496	9	420	120
PR02-106	0.6360	0.0290	0.0836	0.0014	0.0556	0.0026	496	18	518	8	341	98
PR02-107	0.7560	0.0280	0.0924	0.0016	0.0594	0.0023	569	16	570	9	534	88
PR02-108	0.7550	0.0420	0.0884	0.0018	0.0616	0.0034	562	25	546	10	540	120
PR02-109	0.6360	0.0500	0.0808	0.0018	0.0572	0.0045	487	31	501	11	360	170
PR02-110	0.6370	0.0270	0.0793	0.0012	0.0577	0.0024	494	17	492	7	444	90
PR02-111	0.6560	0.0330	0.0837	0.0015	0.0579	0.0031	509	21	518	9	410	110
PR02-112	0.7810	0.0470	0.0951	0.0018	0.0610	0.0040	572	27	586	11	460	130

Table 5 Laser ablation ICP-MS U–Pb isotopic data of detrital zircons from sample PR04

Analysis	Isotopic ratios						Calculated ages Ma					
	$^{207}Pb/^{235}U$	±2 sigma	$^{206}Pb/^{238}U$	±2 sigma	$^{207}Pb/^{206}Pb$	±2 sigma	$^{207}Pb/^{235}U$	±2 sigma	$^{206}Pb/^{238}U$	±2 sigma	$^{207}Pb/^{206}Pb$	±2 sigma
PR04-2	0.6570	0.0340	0.0821	0.0013	0.0581	0.0032	505	21	508	8	433	120
PR04-3	15.6400	0.5600	0.5559	0.0084	0.2025	0.0082	2852	34	2849	35	2840	65
PR04-4	0.8660	0.0560	0.0997	0.0021	0.0624	0.0041	625	31	612	12	610	140
PR04-5	0.7870	0.0350	0.0955	0.0013	0.0593	0.0028	585	20	588	8	522	110
PR04-6	0.7170	0.0400	0.0905	0.0014	0.0574	0.0035	545	24	558	8	480	140
PR04-7	7.1900	0.2500	0.3911	0.0051	0.1332	0.0053	2135	31	2127	24	2121	68
PR04-8	0.5970	0.0310	0.0746	0.0011	0.0579	0.0033	473	19	464	7	470	120
PR04-9	0.6240	0.0290	0.0786	0.0011	0.0572	0.0029	489	18	488	7	449	110
PR04-10	0.6430	0.0400	0.0800	0.0013	0.0580	0.0038	498	25	496	8	430	140
PR04-11	0.8030	0.0380	0.0958	0.0014	0.0604	0.0031	593	21	590	8	563	110
PR04-12	0.7480	0.0400	0.0899	0.0018	0.0596	0.0034	567	22	555	10	560	120
PR04-13	1.2550	0.0690	0.1327	0.0024	0.0691	0.0040	819	32	803	13	800	120
PR04-15	0.6540	0.0470	0.0833	0.0015	0.0567	0.0042	502	29	516	9	380	150
PR04-16	0.6040	0.0270	0.0775	0.0011	0.0562	0.0027	478	17	481	7	422	110
PR04-17	0.6250	0.0330	0.0782	0.0012	0.0576	0.0033	488	21	485	7	444	120
PR04-18	0.7950	0.0480	0.0944	0.0017	0.0617	0.0041	586	28	581	10	530	140
PR04-19	0.7260	0.0750	0.0857	0.0024	0.0612	0.0065	544	43	530	14	520	220
PR04-20	0.8300	0.0440	0.0970	0.0016	0.0617	0.0036	608	25	597	9	600	130
PR04-21	6.8500	0.2300	0.3821	0.0051	0.1283	0.0048	2093	28	2086	24	2075	72
PR04-23	0.8350	0.0820	0.0982	0.0025	0.0619	0.0065	603	46	604	15	530	220
PR04-26	9.7600	0.3200	0.4281	0.0066	0.1641	0.0060	2410	30	2297	30	2500	57
PR04-27	0.7460	0.0300	0.0885	0.0011	0.0606	0.0026	564	17	547	6	601	96
PR04-30	0.6210	0.0420	0.0772	0.0015	0.0583	0.0041	483	26	479	9	460	150
PR04-31	0.6000	0.0380	0.0773	0.0014	0.0563	0.0038	471	25	480	8	370	140
PR04-34	0.8400	0.0300	0.0989	0.0011	0.0613	0.0025	617	17	608	6	621	87
PR04-35	4.9200	0.3000	0.3219	0.0080	0.1122	0.0074	1772	53	1796	39	1720	130
PR04-38	11.6800	0.3600	0.4612	0.0058	0.1834	0.0067	2575	29	2444	26	2676	60
PR04-40	0.6390	0.0430	0.0779	0.0016	0.0595	0.0044	497	26	483	9	500	150
PR04-42	0.6660	0.0550	0.0811	0.0019	0.0590	0.0048	514	34	503	12	510	180
PR04-50	0.6690	0.0510	0.0822	0.0020	0.0591	0.0043	514	31	509	12	500	160
PR04-59	13.5200	0.5300	0.5235	0.0095	0.1872	0.0081	2700	37	2710	40	2684	74
PR04-60	9.0000	0.3200	0.4125	0.0061	0.1580	0.0066	2334	33	2225	28	2420	72
PR04-72	5.4500	0.1800	0.3358	0.0046	0.1168	0.0046	1888	29	1866	22	1905	68
PR04-83	0.6660	0.0760	0.0857	0.0022	0.0550	0.0062	496	46	530	13	260	220

Table 5 (continued)

Analysis	Isotopic ratios						Calculated ages Ma					
	$^{207}Pb/^{235}U$	±2 sigma	$^{206}Pb/^{238}U$	±2 sigma	$^{207}Pb/^{206}Pb$	±2 sigma	$^{207}Pb/^{235}U$	±2 sigma	$^{206}Pb/^{238}U$	±2 sigma	$^{207}Pb/^{206}Pb$	±2 sigma
PR04-96	6.5600	0.2700	0.3770	0.0064	0.1258	0.0056	2048	38	2061	30	2020	84
PR04-112	0.6270	0.0280	0.0802	0.0011	0.0567	0.0028	491	18	497	6	414	110
PR04-1	1.2090	0.0840	0.1292	0.0026	0.0692	0.0050	793	39	783	15	700	150
PR04-1-1	0.6360	0.0300	0.0813	0.0012	0.0569	0.0027	494	19	504	7	401	100
PR04-4-1	0.6320	0.0290	0.0789	0.0011	0.0580	0.0026	495	18	490	7	486	100
PR04-5-1	0.6490	0.0300	0.0822	0.0012	0.0573	0.0026	505	19	509	7	442	97
PR04-6-1	0.7530	0.0500	0.0949	0.0017	0.0574	0.0038	561	30	585	10	410	140
PR04-7-1	0.6230	0.0370	0.0781	0.0014	0.0584	0.0035	488	24	485	9	430	130
PR04-8-1	0.8170	0.0350	0.0980	0.0013	0.0605	0.0026	602	20	603	8	558	95
PR04-9-1	6.5510	0.1900	0.3633	0.0043	0.1307	0.0035	2052	25	1997	20	2099	47
PR04-10-1	0.6220	0.0320	0.0779	0.0012	0.0579	0.0030	487	20	484	7	460	110
PR04-11	1.0360	0.0740	0.1162	0.0024	0.0651	0.0048	704	37	708	14	610	150
PR04-12	0.8910	0.0340	0.1044	0.0013	0.0618	0.0023	643	18	640	8	613	79
PR04-13	0.6490	0.0340	0.0814	0.0012	0.0577	0.0030	504	21	504	7	460	110
PR04-14	11.6300	0.3300	0.4562	0.0060	0.1847	0.0051	2575	28	2422	26	2695	46
PR04-15	0.7970	0.0430	0.0983	0.0017	0.0584	0.0031	589	25	605	10	470	110
PR04-19	0.6480	0.0330	0.0820	0.0013	0.0572	0.0028	502	21	508	8	414	110
PR04-20	0.7200	0.0360	0.0900	0.0013	0.0581	0.0028	543	21	556	8	436	100
PR04-21	0.7320	0.0570	0.0899	0.0024	0.0599	0.0052	551	34	555	14	490	180
PR04-22	0.8680	0.0450	0.1009	0.0015	0.0621	0.0032	631	25	620	9	630	120
PR04-23	1.1100	0.1200	0.1153	0.0035	0.0687	0.0072	729	57	703	21	700	230
PR04-26	11.5300	0.4000	0.4550	0.0072	0.1837	0.0061	2562	32	2417	32	2674	55
PR04-27	0.9690	0.0360	0.1041	0.0014	0.0674	0.0025	685	19	638	8	819	76
PR04-28	0.6470	0.0310	0.0809	0.0011	0.0579	0.0028	500	19	501	7	434	100
PR04-29	0.7680	0.0560	0.0946	0.0019	0.0589	0.0044	559	33	582	11	370	150
PR04-30	0.6330	0.0260	0.0788	0.0011	0.0584	0.0025	495	16	489	7	488	92
PR04-31	0.7580	0.0290	0.0933	0.0012	0.0587	0.0022	570	16	575	7	512	78
PR04-33	7.1100	0.2300	0.3900	0.0056	0.1326	0.0043	2126	30	2122	26	2122	57
PR04-34	5.2800	0.2200	0.3302	0.0056	0.1159	0.0046	1856	36	1838	27	1875	71
PR04-35	5.6400	0.2200	0.3440	0.0054	0.1182	0.0042	1915	33	1905	26	1917	68
PR04-36	0.7660	0.0380	0.0927	0.0015	0.0599	0.0029	572	22	571	9	543	100
PR04-37	0.8150	0.0360	0.0965	0.0015	0.0609	0.0026	601	20	594	9	586	95
PR04-38	4.9000	0.1900	0.3075	0.0052	0.1153	0.0043	1799	33	1728	26	1874	67
PR04-40	0.6370	0.0390	0.0794	0.0014	0.0579	0.0036	492	24	492	9	420	130
PR04-41	5.5300	0.2400	0.3419	0.0067	0.1179	0.0051	1899	37	1894	32	1888	75

Table 5 (continued)

Analysis	Isotopic ratios						Calculated ages Ma					
	$^{207}Pb/^{235}U$	±2 sigma	$^{206}Pb/^{238}U$	±2 sigma	$^{207}Pb/^{206}Pb$	±2 sigma	$^{207}Pb/^{235}U$	±2 sigma	$^{206}Pb/^{238}U$	±2 sigma	$^{207}Pb/^{206}Pb$	±2 sigma
PR04-43	5.5500	0.1800	0.3470	0.0047	0.1159	0.0036	1905	28	1920	23	1886	55
PR04-44	5.3610	0.1700	0.3108	0.0041	0.1248	0.0036	1875	26	1744	20	2023	49
PR04-45	0.6460	0.0350	0.0807	0.0013	0.0579	0.0031	497	22	501	8	413	110
PR04-46	0.6780	0.0310	0.0848	0.0013	0.0579	0.0026	523	19	525	8	483	99
PR04-47	11.6000	0.5700	0.4827	0.0110	0.1748	0.0083	2552	46	2535	48	2568	79
PR04-48	0.6490	0.0280	0.0803	0.0011	0.0587	0.0026	506	17	498	7	515	97
PR04-49	9.4300	0.2800	0.4305	0.0056	0.1584	0.0046	2375	28	2307	25	2424	50
PR04-51	0.6430	0.0320	0.0798	0.0014	0.0585	0.0029	500	20	495	8	484	110
PR04-52	0.6370	0.0330	0.0802	0.0013	0.0574	0.0030	495	20	497	8	440	110
PR04-53	0.6370	0.0250	0.0814	0.0011	0.0566	0.0022	497	16	504	7	419	85
PR04-55	0.7900	0.0330	0.0957	0.0016	0.0595	0.0024	588	19	589	9	551	90
PR04-56	0.7390	0.0400	0.0907	0.0016	0.0588	0.0031	552	23	559	9	460	110
PR04-57	0.6050	0.0280	0.0767	0.0011	0.0571	0.0025	478	18	476	6	432	95
PR04-58	0.6240	0.0300	0.0796	0.0012	0.0560	0.0025	486	19	494	7	392	99
PR04-59	0.8880	0.0680	0.1020	0.0022	0.0642	0.0049	619	38	626	13	500	160
PR04-61	5.6000	0.2200	0.3423	0.0064	0.1183	0.0046	1909	36	1897	31	1912	73
PR04-64	6.2500	0.1900	0.3644	0.0054	0.1246	0.0036	2013	29	2002	25	2016	51
PR04-65	0.7730	0.0450	0.0927	0.0017	0.0611	0.0036	576	27	572	10	510	120
PR04-66	0.7770	0.0570	0.0913	0.0020	0.0620	0.0047	576	33	563	12	570	170
PR04-67	0.7180	0.0360	0.0867	0.0013	0.0601	0.0030	543	21	536	8	517	110
PR04-68	0.8780	0.0380	0.1053	0.0015	0.0602	0.0026	633	21	645	9	539	93
PR04-71	0.755	0.052	0.0892	0.0017	0.0617	0.0042	556	30	550.5	9.9	480	140
PR04-73	0.765	0.03	0.0919	0.0012	0.0602	0.0023	574	17	566.7	7.2	573	83
PR04-75	6.88	0.23	0.3816	0.0054	0.1299	0.0041	2086	30	2082	25	2077	56

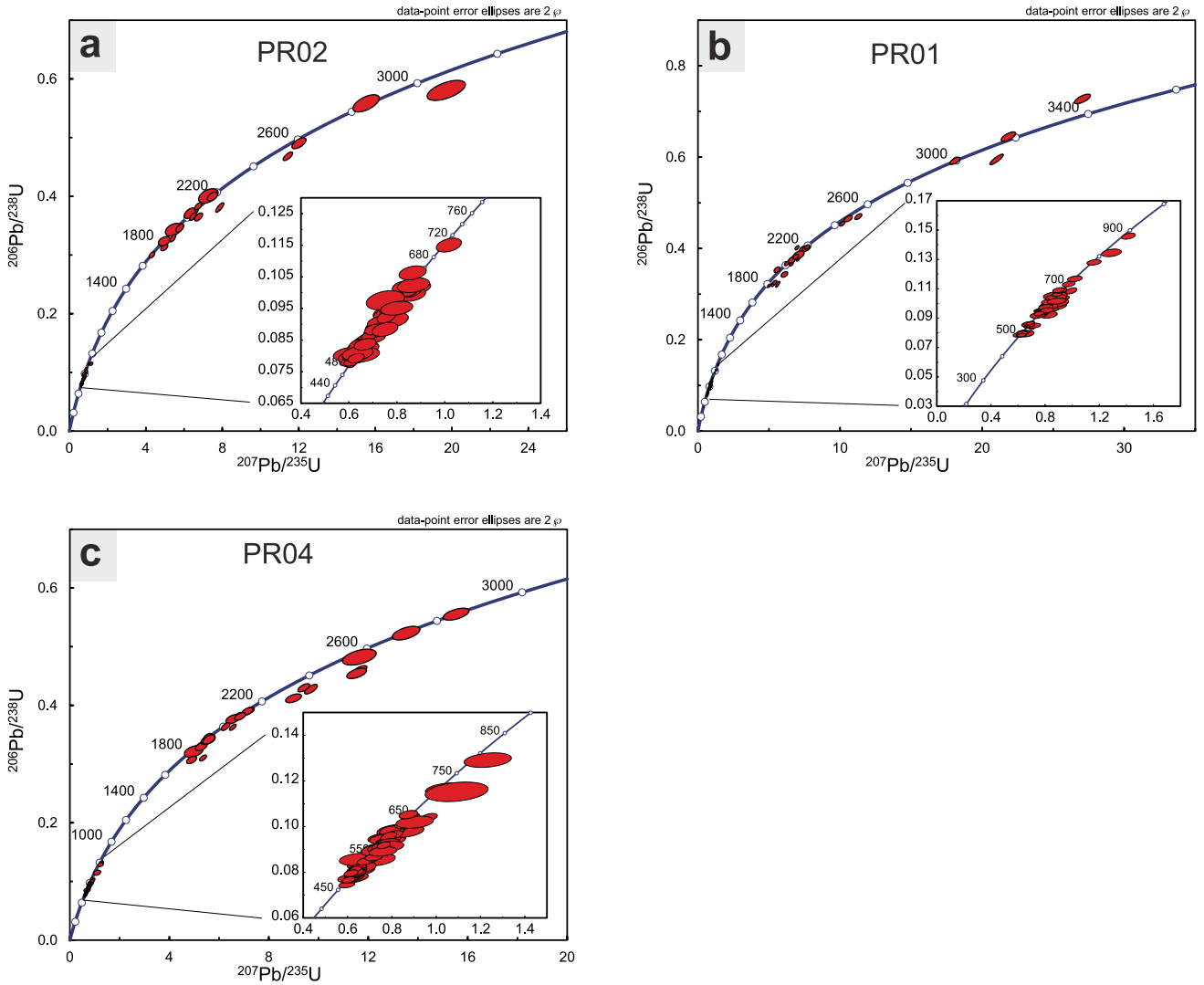

Fig. 6 U–Pb Concordia diagrams for samples from the Bystrzyckie Mts. Concordia plots were done using the Isoplot/Ex 4.15 Excel add-in (Ludwig 2008)

this sample (McLennan et al. 1993). This clearly indicates that the Bystrzyckie Mts. quartzites cannot represent rhyolites or tuffs, as suggested by Jastrzębski et al. (2016) for the Goszów quartzite exposed in the eastern part of the Orlica-Śnieżnik dome. This is also supported by morphology of the youngest zircons that closely resemble those in the Śnieżnik orthogneiss and are strikingly different from those documented in local metaryolites from the Gniewoszów area (Mazur et al. 2015). However, we do not exclude the possibility of some minor syn-sedimentary volcanic input but, if at all present, it was volumetrically minor.

Various diagrams are available to identify the tectonic setting of a source region and were successfully used in the numerous studies (e.g. Bhatia 1983; Roser and Korsch 1986). Because in the case of metamorphosed rock successions discrimination of tectonic setting of a sedimentary basin should rely on immobile trace elements, we first utilized the Ti/Zr vs. La/Sc diagram and Sc–Th–Zr ternary plot of Bhatia and Crook (1986). These plots show that the analysed samples display trace element composition typical of sediments deposited on a continental passive margin (Fig. 8c, d). Despite potential mobility of the major elements, we also explored a diagram of Roser and Korsch (1986) devised to determine the tectonic setting of terrigenous sedimentary rocks utilising K_2O/Na_2O ratio and SiO_2 abundance. In this plot, the studied samples fall within the field of the passive margin sediments (Fig. 8e). Recently, Verma and Armstrong-Altrin (2013) proposed two new discriminant functions based on major elements for the tectonic discrimination of siliciclastic sediments from three main tectonic settings including island or continental arc, continental rift and collision zone. Verma and Armstrong-Altrin (2013)

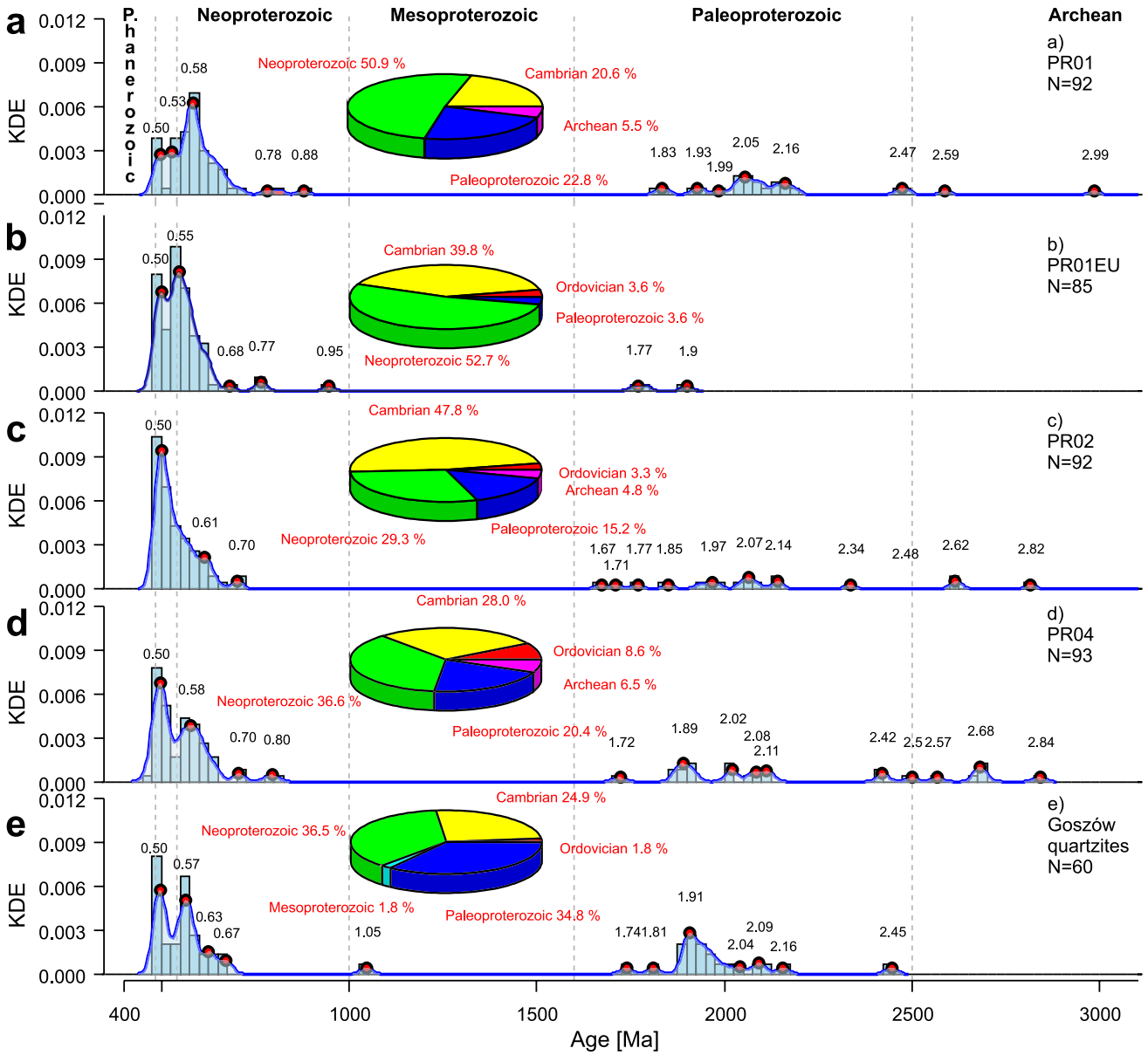

Fig. 7 Binned frequency-density plots of detrital zircons from: **a–d** analyzed samples (*N* number of analyses) with marked major zircon forming events (see text for details); **e** Goszów quartzites (Mazur et al. 2012). For zircons older than 1 Ga $^{207}Pb/^{206}Pb$ ages were taken for interpretation and the $^{206}Pb/^{238}U$ ages were utilised for younger grains. Frequency-density plots were designed via the R software environment (R Core Team 2012)

suggest that the discriminant functions are insensitive to element mobility. Indeed, investigated quartzite display values of mentioned discriminant functions typical of rift-related sandstones demonstrating the usefulness of this technique even for metamorphosed rock suites (Fig. 8f).

Time of deposition

The youngest zircon population documented in the studied quartzites defines a prominent density peak at 500 Ma (Figs. 6, 7, 9a; Tables 2, 3, 4, 5). Assuming no significant Pb-loss in this population, it is our best estimate of the maximum deposition age. Although in the sample PR04 we observed three crystals younger than 480 Ma, they were not reproduced in other samples and taking into account their paucity, their young age is likely to be caused by the partial Pb-loss.

Our estimate is in broad agreement with U–Pb detrital zircon and monazite ages for the Goszów quartzite whose max. deposition age was estimated as ca. 490–494 Ma (Mazur et al. 2012; Jastrzębski et al. 2016). However, the youngest zircon grains reported by Jastrzębski et al. (2010)

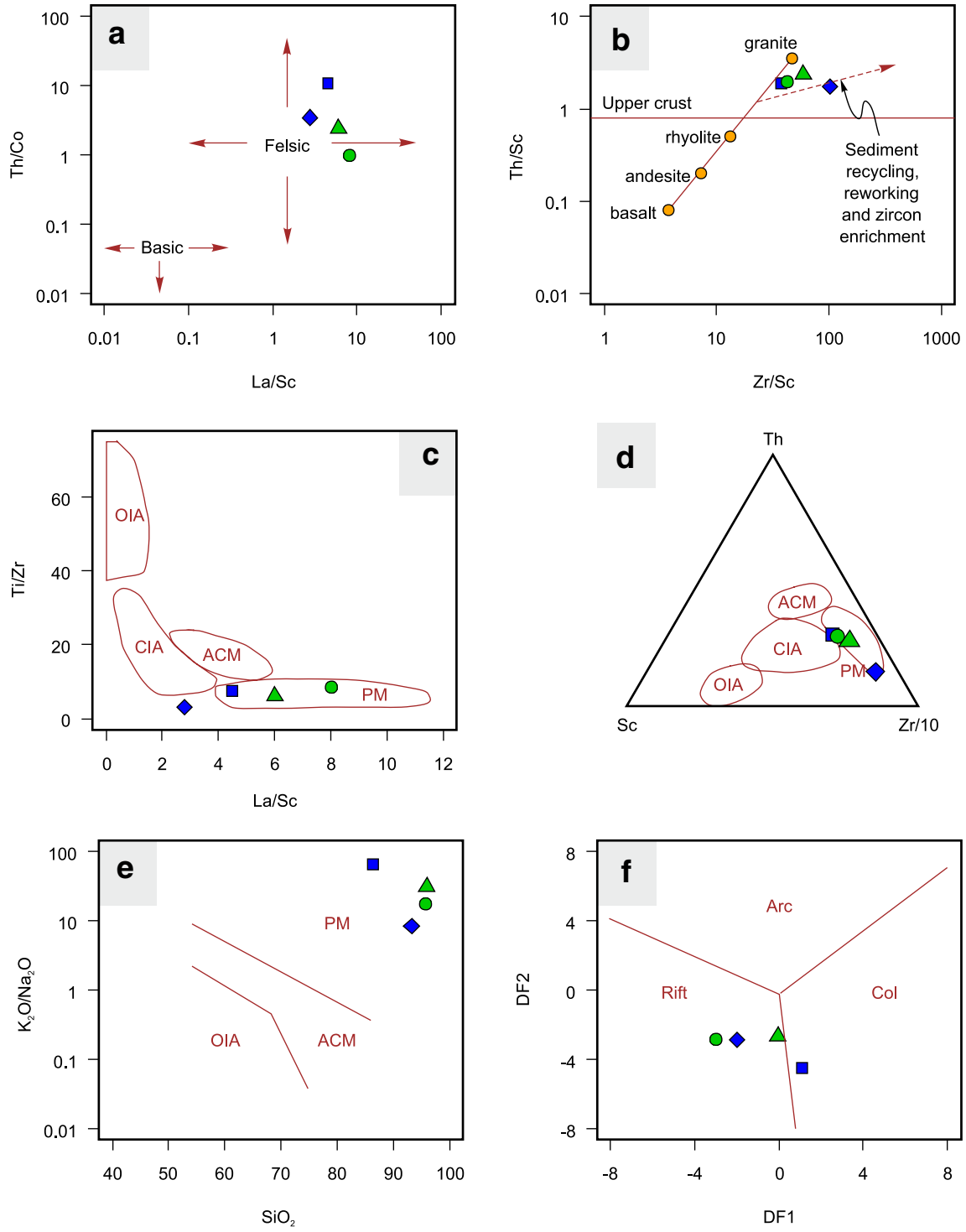

Fig. 8 Diagrams illustrating: **a** lithology of the source area after Cullers (2002), **b** the influence of sediment recycling and zircon enrichment on chemical composition of the investigated quartzites after McLennan et al. (1993), **c**, **d** discrimination diagrams showing tectonic setting of deposition of the protolith to the Bystrzyckie quartzites. (diagrams after Bhatia and Crook 1986). *PM* passive margin, *CIA* continental island arc, *ACM* active continental margin, *OIA* oceanic island arc. **e** SiO_2 versus K_2O/Na_2O diagram of Roser and Korsch (1986), **f** discriminant-function multi-dimensional diagram after Verma and Armstrong-Altrin (2013). Samples fall in or near field typical of rift-related sandstones. Symbols as in Fig. 4

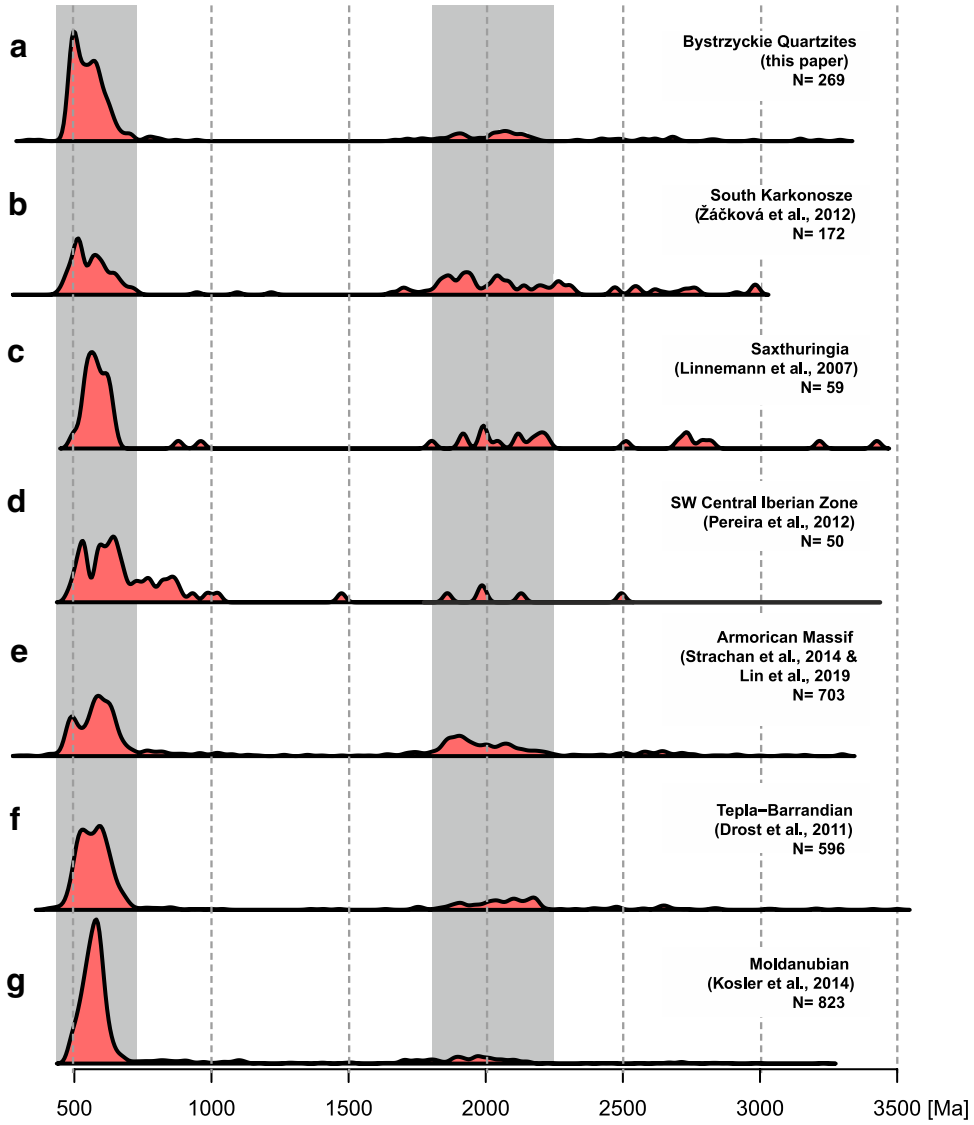

Fig. 9 Kernel density plots for detrital zircons from Early Ordovician quartzites from: **a** the Bystrzyckie Mts (this paper), **b** South Karkonosze (Žáčková et al. 2010), **c** Saxothuringian Zone (Linnemann et al. 2007), **c** Armorican Massif (Strachan et al. 2014; Lin et al. 2019), **d** SW Central Iberian Zone (Pereira et al. 2012), **e** Armorican Massif (Strachan et al. 2014; Lin et al. 2019), **f** Teplá-Barrandian Zone (Drost et al. 2011) and **g** Molnadubian Zone (Košler et al. 2014). *N* number of analyzed grains. The grey shading highlights the bimodal distribution of detrital zircon ages common for all units. Kernel density plots were designed via the R software environment (R Core Team 2012)

with ages of 460–470 Ma most probably suffered significant Pb-loss. These ages are younger than any reported zircons from the Śnieżnik orthogneiss or even metarhyolites exposed in the Orlica-Śnieżnik dome rocks which are the most probable source of detritus for the investigated quartzites (e.g. Turniak et al. 2000; Kröner et al. 2001; Lange et al. 2002; Mazur et al. 2015).

Provenance constraints

The Neoproterozoic Avalonian-Cadomian belt was formed due to long-lasting Andean-type orogeny as a relatively large magmatic arc spreading over several thousand kilometres along the northern margin of the Gondwana. It extended from the Amazonia in the West, through the West African Craton and the Saharan Metacraton to the Arabian-Nubian shield in the East (e.g. von Raumer et al. 2002). As these cratonic domains bear a record of numerous tectonomagmatic events responsible for the zircon formation it may allow for describing the palaeogeographic position of individual terranes within this long arc. Figures 9 and 10 show the age ranges of the magmatic-metamorphic units encountered in several cratonic areas as well as in the Early Ordovician quartzites known from other Cadomian terranes that are now exposed in the Variscan Belt of Europe. Comparison of zircon age spectra of various crustal domains with the presented zircon age spectra obtained for the investigated quartzites from the Bystrzyckie Mts. allows a conclusion concerning the provenance of the detritus comprised within the Bystrzyca-Orlica massif.

The youngest age spectra documented in the quartzites from the Bystrzyca-Orlica massif are typical of the Cambro-Ordovician sedimentary successions covering Cadomian terranes known from other parts of the Variscan Belt of

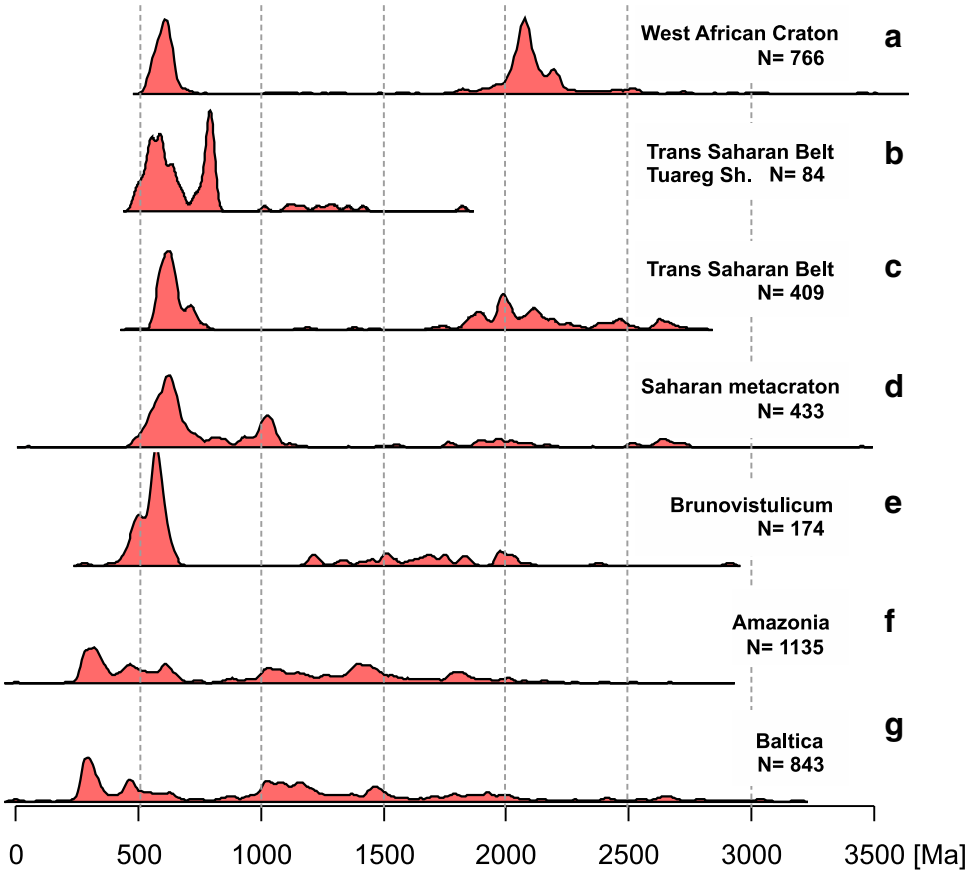

Fig. 10 Kernel density plots for detrital zircons from: **a** West African Craton (Abati et al. 2010), **b** Trans-Saharan Belt–Tuareg Shield (Henry et al. 2009), **c** Trans-Saharan Belt (Peucat et al. 2003; Abdallah et al. 2007; Bendaoud et al. 2008; Bosch et al. 2016), **d** Saharan Metacraton (Meinhold et al. 2011), **e** Brunovistulicum (Friedl et al. 2004; Mazur et al. 2010), **f** Amazonian Craton (Gaucher et al. 2008; Geraldes et al. 2014; Pankhurst et al. 2016), **g** Baltica (Valverde-Vaquero et al. 2000; Kristoffersen et al. 2014; Kuznetsov et al. 2014). Kernel density plots were designed via the R software environment (R Core Team 2012)

Europe (Fig. 9). This Cambro-Ordovician cover comprises: (1) quartzite lenses exposed in the southern part of the Karkonosze-Izera massif interpreted as the eastern extension of the Saxothuringian zone where the youngest population of zircons shows a peak at ca. 500 Ma (Žáčková et al. 2010), (2) metaconglomerate of the Langer Berg Formation in the Saxothuringian Zone with the youngest zircons ranging from 485 to 500 Ma (Linnemann et al. 2007), and (3) the Armorican quartzite exposed in the Armorican Massif as well as in the Iberian Massif excluding the South Portuguese Zone (e.g. Strachan et al. 2014). The Armorican quartzite of the Iberian Massif displays a Concordia age of the youngest zircons at 522 ± 7 Ma (e.g. Linnemann et al. 2008; Fernández-Suárez et al. 2002a, b). It is worth to note that also other Neoproterozoic and Cambro-Ordovician siliciclastic sedimentary successions exposed in the Teplá-Barrandian and Moldanubian Zones show very similar detrital zircon age spectra indicating similar provenance (Fig. 9f, g; Drost et al. 2011; Košler et al. 2014). The only important exceptions can be noticed for quartzites exposed in the SW central part of the Iberian Zone. These rocks bear a significant admixture of zircons revealing c. 1 Ga typifying Grenvillian crust and thus interpreted as derived from erosion of the Arabian-Nubian Shield (Fig. 9d; e.g., Pereira et al. 2012; Fernández-Suárez et al. 2014).

The youngest population of zircon grains recognised in the analysed quartzites from the Orlica-Śnieżnik dome were probably derived by erosion of Cambro-Ordovician granites widely exposed in the Saxothuringian zone. These metagranites are represented by e.g. orthogneiss from the Erzgebirge (Tichomirowa et al. 2001; Košler et al. 2004; Mingram et al. 2004), the Rumburk granite from the Izera-Karkonosze Massif (Oliver et al. 1993; Oberc-Dziedzic et al. 2009, 2010; Zieger et al. 2017), the Milchberg granite from the Torgau-Doberlug Syncline (Linnemann et al. 2007) or the Śnieżnik orthogneiss from the Orlica-Śnieżnik dome (e.g. Oliver et al. 1993; Turniak et al. 2000; Kröner et al. 2001; Lange et al. 2005). Neoproterozoic euhedral grains might have been derived from the granitoid intrusions dated at c. 540 Ma that were reported from: (1) Wądroże Wielkie located on the Fore-Sudetic Block (Żelaźniewicz et al. 2004), (2) Lausitz granitoid, Glasbach and Laubach granites or Dohna granodiorite exposed in the Saxothurignian zone (Linnemann and Heuse 2001) and (3) orthogneisses reported from Erzgebirge (Tichomirowa et al. 2001; Mingram et al. 2004). Consequently, the presence of Cambro-Ordovician and Neoproterozoic euhedral zircons preserved in the quartzite lenses from the Bystrzyckie Mts. suggest a relatively short distance of transport before deposition of these rocks and, consequently, a local source of the detritus.

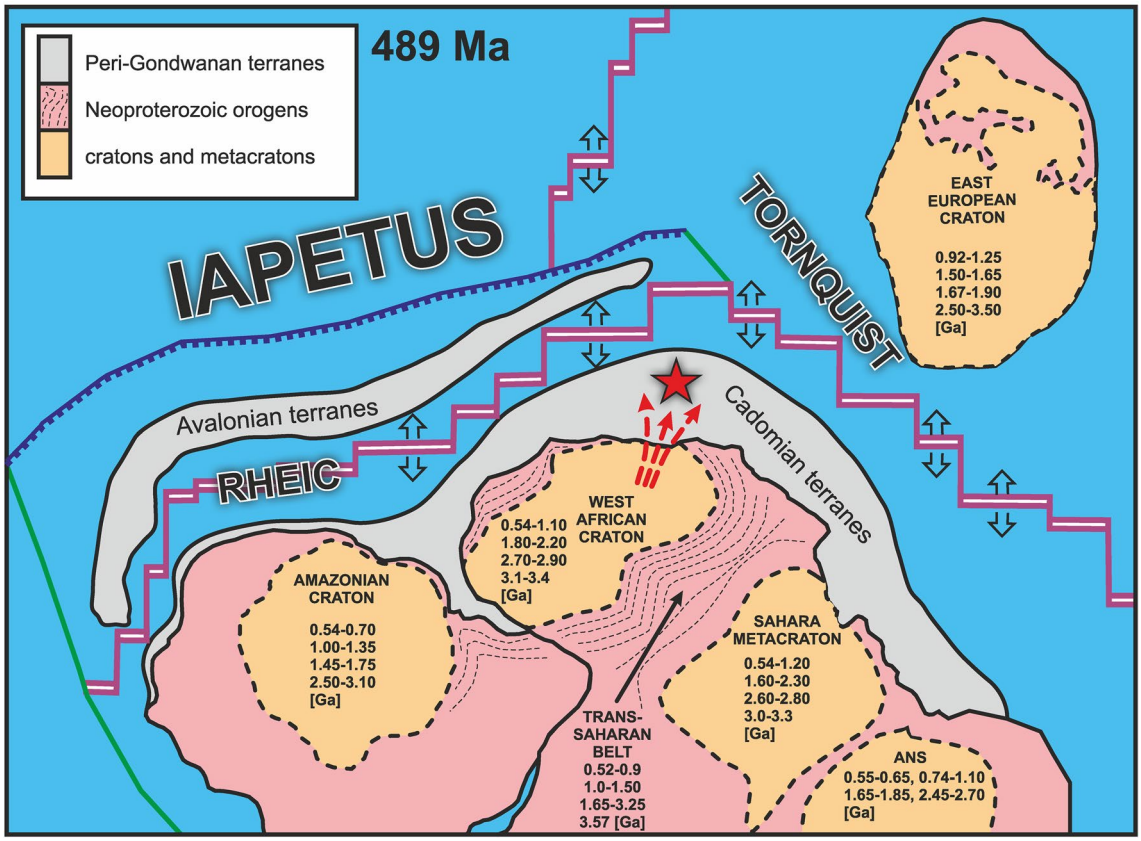

Fig. 11 Tentative simplified reconstruction of Western Gondwana during the Early Ordovician, modified after Domeier (2016) and Torsvik (2017). Ages of main zircon forming events for Amazonian Craton, West African Craton and Saharan Metacraton after Albert et al. (2015). Ages of main zircon forming events for East European Craton after Kristoffersen et al. (2014). References for Trans-Saharan Belt as in Fig. 10b. *ANS* Arabian-Nubian Shield. Red star marks the position of the metaquartzite sink area within the Cadomian arc. Red arrows indicate the main direction of sedimentary transport. Types of lithosperic boundaries: magenta—spreading ridge, blue—subduction, green—transform

This is in line with the observed weak mechanical abrasion of the investigated euhedral zircons. However, a group of Neoproterozoic zircons is characterized by ovoid, strongly rounded shapes due to relatively intense mechanical abrasion (Fig. 5). The presence of such grains indicates recycling by transport from (volcano)-sedimentary successions, possibly from the Stronie (532 ± 6 Ma) and Młynowiec formations (563 ± 6 Ma) in the Orlica-Śnieżnik dome (Mazur et al. 2012, 2015), from the Zwethau (534 Ma) and the Rothstein (565–570 Ma) formations in the Saxohuringian zone (e.g. Elicki 1997; Linnemann 2007) or from glaciomarine sedimentary rocks documented in the Elbe zone and the North Saxon antiform in the southeastern part of the Saxothuringian zone with the youngest detrital zircon populations showing ages of 562–565 Ma (Linnemann et al. 2018). Moreover, LA-ICP-MS U–Pb detrital zircon data from Early–Middle Cambrian strata of the Torgau-Doberlug Syncline from the Saxothuringian zone show Cadomian and older zircons in this area (Abubaker et al. 2017). Consequently, anhedral Neoproterozoic zircons documented in the studied quartzites may represent recycled material delivered through local sedimentary successions.

Presented detrital zircon age spectra indicate that there was a period of magmatic quiescence between 0.9 and 1.7 Ga in the source area as there are only few zircon grains of this age documented in the investigated quartzites (Figs. 6, 7, 9). The same age gap in the zircon age spectra is also reported from domains like the West African Craton and the Trans-Saharan Belt (Fig. 10a, c). However, the Trans-Saharan Belt might be excluded as a potential source of detrital material for the investigated quartzite samples due to occurrence of Mesoproterozoic zircons in some parts of this crustal domain. In addition, the Saharan Metacraton, Amazonia, Baltica, Avalonia and Brunovistulicum may also be excluded as a potential source of detritus since these cratonic areas are characterized by the existence of Mesoproterozoic zircons (Fig. 10c–g).

Summing up, we suggest that the data presented here indicate that up to the Early Ordovician rock successions exposed in the Orlica-Śnieżnik dome were part of the

Saxo-Thuringia and must have been located close to the West African Craton (Fig. 11). The latter together with the supracrustal successions and magmatic complexes of the Cadomian terranes served as the source for the detritus. Available detrital zircon ages from Cambro-Ordovician sedimentary successions covering Saxo-Thuringia, Teplá-Barrandian and Moldanubian Zones as well as the Armorican Massif clearly indicate that all these Neoproterozoic crustal fragments were sourced from the same cratonic areas and Cadomian arc-related basement located at the northern periphery of Gondwana (Figs. 9, 10; e.g. Linnemann and Romer 2002; Pastor-Galán et al. 2013). Consequently, we support suggestions that during the Cambro-Ordovician Cadomian crustal fragments were dispersed along the northern periphery of Gondwana most probably defining an extended shelf set on a passive continental margin (Žák and Sláma 2018).

Conclusions

The quartzite from the western part of the Orlica-Śnieżnik dome (the Bystrzyckie Mts.) provides new input to understand the pre-Variscan history of the Cadomian crust cropping out in the Central Sudetes. Bulk rock chemistry and detrital zircon age spectra obtained using LA ICP-MS U–Pb show that these rocks represent the same though dismembered lithostratigraphic horizon equivalent to the Goszów quartzite exposed in the eastern part of the Orlica-Śnieżnik dome in the Śnieżnik massif. The youngest zircons with a Late Cambrian density peak providing the maximum depositional age of c. 500 Ma, were delivered by the erosion of granitoids with protolith ages of c. 517–490 Ma attesting a relatively short distant transport before deposition of the quartzite. Obtained zircon age spectra resemble that documented in the Neoproterozoic (meta)sedimentary and (meta) magmatic rocks exposed in the eastern part of the Orlica-Śnieżnik dome as well as elsewhere in the Saxothuringian zone. Consequently, presented data point to Saxothuringian affinity of the volcano-sedimentary successions exposed in the western part of the Orlica-Śnieżnik dome. Bulk rock geochemistry suggests that the quartzite represents a highly mature quartz-rich sandstones deposited on the passive Gondwana margin.

Acknowledgements The research of JS, KT and PR was funded by the University of Wrocław Grant No 0401/1017/18 zad. 3. RA acknowledges financial support by grants from the Polish Academy of Sciences. We are grateful to Ewa Teper (University of Silesia in Katowice) for help with CL imaging. Valuable comments from Ulf Linnemann and Arne Willner greatly improved this paper. Editorial handling of the paper by Wolf-Christian Dullo is highly appreciated.

References

Abati J, Aghzer AM, Gerdes A, Ennih N (2010) Detrital zircon ages of Neoproterozoic sequences of the Moroccan Anti-Atlas belt. Precambr Res 181:115–128. https://doi.org/10.1016/j.precamres.2010.05.018

Abdallah N, Liégeois J-P, De Waele B, Fezaa N, Ouabadi A (2007) The Temaguessine Fe-cordierite orbicular granite (Central Hoggar, Algeria): U–Pb SHRIMP age, petrology, origin and geodynamical consequences for the late Pan-African magmatism of the Tuareg shield. J Afr Earth Sci 49:153–178. https://doi.org/10.1016/j.jafrearsci.2007.08.005

Abubaker A, Hofmann M, Gärtner A, Linnemann U, Elicki O (2017) First U–Pb geochronology on detrital zircons from Early-Middle Cambrian strata of the Torgau-Doberlug Syncline (eastern Germany) and palaeogeographic implications. Int J Earth Sci 106:2445–2459. https://doi.org/10.1007/s00531-016-1440-y

Albert R, Arenas R, Gerdes A, Sánchez Martínez S, Fernández-Suárez J, Fuenlabrada JM (2015) Provenance of the Variscan Upper Allochthon (Cabo Ortegal Complex, NW Iberian Massif). Gondwana Res 28:1434–1448. https://doi.org/10.1016/j.gr.2014.10.016

Anczkiewicz AA, Anczkiewicz R (2016) U–Pb zircon geochronology and anomalous Sr–Nd–Hf isotope systematics of late orogenic andesites: Pieniny Klippen Belt, Western Carpathians, South Poland. Chem Geol 427:1–16. https://doi.org/10.1016/j.chemgeo.2016.02.004

Baier J, Audétat A, Keppler H (2008) The origin of the negative niobium tantalum anomaly in subduction zone magmas. Earth Planet Sci Lett 267:290–300. https://doi.org/10.1016/j.epsl.2007.11.032

Bandres A, Eguiluz L, Gil Ibarguchi JI, Palacios T (2002) Geodynamic evolution of a Cadomian arc region: the northern Ossa-Morena zone, Iberian massif. Tectonophysics 352:105–120. https://doi.org/10.1016/S0040-1951(02)00191-9

Bendaoud A, Ouzegane K, Godard G, Liégeois J-P, Kienast J-R, Bruguier O, Drareni A (2008) Geochronology and metamorphic P–T–X evolution of the Eburnean granulite-facies metapelites of Tidjenouine (Central Hoggar, Algeria): witness of the LATEA metacratonic evolution. Geol Soc Lond Spec Publ 297:111–146. https://doi.org/10.1144/SP297.6

Bhatia MR (1983) Plate tectonics and geochemical composition of sandstones. J Geol 91:611–627

Bhatia MR, Crook KAW (1986) Trace element characteristics of graywackes and tectonic setting discrimination of sedimentary basins. Contrib Miner Petrol 92:181–193

Bosch D, Bruguier O, Caby R, Buscail F, Hammor D (2016) Orogenic development of the Adrar des Iforas (Tuareg Shield, NE Mali): New geochemical and geochronological data and geodynamic implications. J Geodyn 96:104–130. https://doi.org/10.1016/j.jog.2015.09.002

Buschmann B, Nasdala L, Jonas P, Linnemann U, Gehmlich M (2001) SHRIMP U–Pb dating of tuff-derived and detrital zircons from Cadomian marginal basin fragments (Neoproterozoic) in the northeastern Saxothuringian Zone (Germany). Neues Jahrb Geol Palaeontol Monatshefte 2001:321–342

Chopin F, Schulmann K, Skrzypek E, Lehmann J, Dujardin JR, Martelat JE, Lexa O, Corsini M, Edel JB, Štípská P, Pitra P (2012) Crustal influx, indentation, ductile thinning and gravity redistribution in a continental wedge: Building a Moldanubian mantled gneiss dome with underthrust Saxothuringian material (European Variscan belt). Tectonics. https://doi.org/10.1029/2011TC002951

Cullers RL (2002) Implications of elemental concentrations for provenance, redox conditions, and metamorphic studies of shales and limestones near Pueblo, CO, USA. Chem Geol 191:305–327. https://doi.org/10.1016/S0009-2541(02)00133-X

Domeier M (2016) A plate tectonic scenario for the Iapetus and Rheic oceans. Gondwana Res 36:275–295. https://doi.org/10.1016/j.gr.2015.08.003

Don J, Dumicz M, Wojciechowska I, Żelaźniewicz A (1990) Lithology and tectonics of the Orlica-Śnieżnik Dome, Sudetes; recent state of knowledge. Neues Jahrb Geol Palaeontol Abh 179:159–188

Drost K, Romer RL, Linnemann U, Fatka O, Kraft P, Marek J (2007) Nd-Sr-Pb isotopic signatures of Neoproterozoic–Early Paleozoic siliciclastic rocks in response to changing geotectonic regimes: A case study from the Barrandian area (Bohemian Massif, Czech Republic). In: Special Paper 423: The Evolution of the Rheic Ocean: From Avalonian-Cadomian Active Margin to Alleghenian-Variscan Collision. Geological Society of America, pp 191–208

Drost K, Gerdes A, Jeffries T, Linnemann U, Storey C (2011) Provenance of Neoproterozoic and early Paleozoic siliciclastic rocks of the Teplá-Barrandian unit (Bohemian Massif): evidence from U–Pb detrital zircon ages. Gondwana Res 19:213–231. https://doi.org/10.1016/j.gr.2010.05.003

Elicki O (1997) Biostratigraphic data of the German Cambrian—present state of knowledge. Freib Forsch C466:155–165

Fernández-Suárez J, Alonso GG, Cox R, Jenner GA (2002a) Assembly of the Armorica microplate: a strike-slip terrane delivery? Evidence from U–Pb Ages Of Detrital Zircons. J Geol 110:619–626. https://doi.org/10.1086/341760

Fernández-Suárez J, Gutiérrez Alonso G, Jeffries TE (2002b) The importance of along-margin terrane transport in northern Gondwana: insights from detrital zircon parentage in Neoproterozoic rocks from Iberia and Brittany. Earth Planet Sci Lett 204:75–88. https://doi.org/10.1016/S0012-821X(02)00963-9

Fernandez-Suarez J, Garcia FD, Jeffries TE, Arenas R, Abati J (2003) Constraints on the provenance of the uppermost allochthonous terrane of the NW Iberian Massif: inferences from detrital zircon U–Pb ages. Terra Nova 15:138–144. https://doi.org/10.1046/j.1365-3121.2003.00479.x

Fernández-Suárez J, Gutiérrez-Alonso G, Pastor-Galán D, Hofmann M, Murphy JB, Linnemann U (2014) The Ediacaran-Early Cambrian detrital zircon record of NW Iberia: possible sources and paleogeographic constraints. Int J Earth Sci 103:1335–1357. https://doi.org/10.1007/s00531-013-0923-3

Finger F, Hanzl P, Pin C, von Quadt A, Steyrer HP (2000) The Brunovistulian; Avalonian Precambrian sequence at the eastern end of the Central European Variscides? Geol Soc Spec Publ 179:103–112

Franke W (1989) Tectonostratigraphic units in the Variscan belt of central Europe. In: Geological Society of America Special Papers. Geological Society of America, pp 67–90

Friedl G, Finger F, Paquette J-L, von Quadt A, McNaughton NJ, Fletcher IR (2004) Pre-Variscan geological events in the Austrian part of the Bohemian Massif deduced from U–Pb zircon ages. Int J Earth Sci 93:802–823

Gaucher C, Finney S, Poire D, Valencia V, Grove M, Blanco G, Pamoukaghlian K, Peral L (2008) Detrital zircon ages of Neoproterozoic sedimentary successions in Uruguay and Argentina: Insights into the geological evolution of the Río de la Plata Craton. Precambr Res 167:150–170. https://doi.org/10.1016/j.precamres.2008.07.006

Geraldes MC, Nogueira C, Vargas-Mattos G, Matos R, Teixeira W, Valencia V, Ruiz J (2014) U–Pb detrital zircon ages from the Aguapeí Group (Brazil): implications for the geological evolution of the SW border of the Amazonian Craton. Precambr Res 244:306–316. https://doi.org/10.1016/j.precamres.2014.02.001

Gonçalves L, Alkmim FF, Pedrosa-Soares AC, Dussin IA, de Valeriano CM, Lana C, Tedeschi M (2016) Granites of the intracontinental termination of a magmatic arc: an example from the Ediacaran Araçuaí orogen, southeastern Brazil. Gondwana Res 36:439–458. https://doi.org/10.1016/j.gr.2015.07.015

Henry B, Liégeois JP, Nouar O, Derder MEM, Bayou B, Bruguier O, Ouabadi A, Belhai D, Amenna M, Hemmi A, Ayache M (2009) Repeated granitoid intrusions during the Neoproterozoic along the western boundary of the Saharan metacraton, Eastern Hoggar, Tuareg shield, Algeria: an AMS and U–Pb zircon age study. Tectonophysics 474:417–434. https://doi.org/10.1016/j.tecto.2009.04.022

Jackson SE, Pearson NJ, Griffin WL, Belousova EA (2004) The application of laser ablation-inductively coupled plasma-mass spectrometry to in situ U–Pb zircon geochronology. Chem Geol 211:47–69. https://doi.org/10.1016/j.chemgeo.2004.06.017

Janoušek V, Farrow CM, Erban V (2006) Interpretation of whole-rock geochemical data in igneous geochemistry; introducing geochemical data toolkit (GCDkit). J Petrol 47:1255–1259

Jastrzębski M, Żelaźniewicz A, Nowak I, Murtezi M, Larionov AN (2010) Protolith age and provenance of metasedimentary rocks in Variscan allochthon units: U/Pb SHRIMP zircon data from the Orlica-Śnieżnik Dome, West Sudetes. Geol Mag 147:416–433

Jastrzębski M, Budzyń B, Stawikowski W (2016) Structural, metamorphic and geochronological record in the Goszów quartzites of the Orlica-Śnieżnik Dome (SW Poland): implications for the polyphase Variscan tectonometamorphism of the Saxothuringian terrane: tectonometamorphic record in quartzites of Saxothuringia, SW Poland. Geol J 51:455–479. https://doi.org/10.1002/gj.2647

Jeřábek P, Konopásek J, Žáčková E (2016) Two-stage exhumation of subducted Saxothuringian continental crust records underplating in the subduction channel and collisional forced folding (Krkonoše-Jizera Mts., Bohemian Massif). J Struct Geol 89:214–229. https://doi.org/10.1016/j.jsg.2016.06.008

Keppie JD, Nance RD, Murphy JB, Dostal J (2003) Tethyan, Mediterranean, and Pacific analogues for the Neoproterozoic-Paleozoic birth and development of peri-Gondwanan terranes and their transfer to Laurentia and Laurussia. Tectonophysics 365:195–219. https://doi.org/10.1016/S0040-1951(03)00037-4

Košler J, Bowes DR, Konopásek J, Míková J (2004) Laser ablation ICPMS dating of zircons in Erzgebirge orthogneisses: evidence for Early Cambrian and Early Ordovician granitic plutonism in the western Bohemian Massif. Eur J Mineral 16:15–22. https://doi.org/10.1127/0935-1221/2004/0016-0015

Košler J, Konopásek J, Sláma J, Vrána S (2014) U–Pb zircon provenance of Moldanubian metasediments in the Bohemian Massif. J Geol Soc 171:83–95. https://doi.org/10.1144/jgs2013-059

Kristoffersen M, Andersen T, Andresen A (2014) U–Pb age and Lu–Hf signatures of detrital zircon from Palaeozoic sandstones in the Oslo Rift, Norway. Geol Mag 151:816–829. https://doi.org/10.1017/S0016756813000885

Kröner A, Jaeckel P, Jegner E, Opletal M (2001) Single zircon ages and whole-rock Nd isotopic systematics of early Palaeozoic granitoid gneisses from the Czech and Polish Sudetes (Jizerske Hory, Krkonose Mountains and Orlice-Sneznik Complex). Int J Earth Sci 90:304–324

Kuznetsov NB, Meert JG, Romanyuk TV (2014) Ages of detrital zircons (U/Pb, LA-ICP-MS) from the Latest Neoproterozoic-Middle Cambrian(?) Asha Group and Early Devonian Takaty Formation, the Southwestern Urals: a test of an Australia-Baltica connection within Rodinia. Precambr Res 244:288–305. https://doi.org/10.1016/j.precamres.2013.09.011

Lange U, Bröcker M, Mezger K, Don J (2002) Geochemistry and Rb-Sr geochronology of a ductile shear zone in the Orlica-Śnieżnik dome (West Sudetes, Poland). Int J Earth Sci 91:1005–1016

Lange U, Bröcker M, Armstrong R, Żelaźniewicz A, Trapp E, Mezger K (2005) The orthogneisses of the Orlica-Śnieżnik complex (West Sudetes, Poland): geochemical characteristics, the importance of pre-Variscan migmatization and constraints on the cooling history. J Geol Soc Lond 162:973–984

Lin W, Faure M, Li X-H, Ji W (2019) Pre-Variscan tectonic setting of the south margin of Armorica: Insights from detrital zircon ages distribution and Hf isotopic composition of the St-Georges-sur-Loire Unit (S. Armorican Massif, France). Tectonophysics 766:340–378. https://doi.org/10.1016/j.tecto.2019.06.015

Linnemann U (2007) Ediacaran rocks from the Cadomian basement of the Saxo-Thuringian Zone (NE Bohemian Massif, Germany); age constraints, geotectonic setting and basin development. Geol Soc Spec Publ 286:35–51

Linnemann U, Heuse T (2001) The Ordovician of the Schwarzburg Anticline: geotectonic setting, biostratigraphy and sequence stratigraphy (Saxo-Thuringian Terrane, Germany). Z Dtsch Geol Ges 151:471–491. https://doi.org/10.1127/zdgg/151/2001/471

Linnemann U, Romer RL (2002) The Cadomian Orogeny in Saxo-Thuringia, Germany; geochemical and Nd-Sr-Pb isotopic characterization of marginal basins with constraints to geotectonic setting and provenance. Tectonophysics 352:33–64

Linnemann U, Gehmlich M, Tichomirowa M, Buschmann B, Nasdala L, Jonas P, Luetzner H, Bombach K (2000) From Cadomian subduction to early Paleozoic rifting; the evolution of Saxo-Thuringia at the margin of Gondwana in the light of single zircon geochronology and basin development (Central European Variscides, Germany). Geol Soc Spec Publ 179:131–153

Linnemann U, Gerdes A, Drost K, Buschmann B (2007) The continuum between Cadomian orogenesis and opening of the Rheic Ocean: Constraints from LA-ICP-MS U–Pb zircon dating and analysis of plate-tectonic setting (Saxo-Thuringian zone, northeastern Bohemian Massif, Germany). Special Paper 423: The Evolution of the Rheic Ocean: From Avalonian-Cadomian Active Margin to Alleghenian-Variscan Collision 423:61–96

Linnemann U, Pereira F, Jeffries TE, Drost K, Gerdes A (2008) The Cadomian Orogeny and the opening of the Rheic Ocean; the diacrony of geotectonic processes constrained by LA-ICP-MS U/Pb zircon dating (Ossa-Morena and Saxo-Thuringian zones, Iberian and Bohemian massifs). Tectonophysics 461:21–43

Linnemann U, Pidal AP, Hofmann M, Drost K, Quesada C, Gerdes A, Marko L, Gärtner A, Zieger J, Ulrich J, Krause R, Vickers-Rich P, Horak J (2018) A ~565 Ma old glaciation in the Ediacaran of peri-Gondwanan West Africa. Int J Earth Sci 107:885–911. https://doi.org/10.1007/s00531-017-1520-7

Ludwig KR (2008) Isoplot/Ex 3.70. A Geochronological Toolkit for Microsoft Excel. Berkeley Geochronological Center

Martínez Catalán JR, Arenas R, Abati J, Martínez SS, García FD, Suárez JF, Cuadra PG, Castiñeiras P, Barreiro JG, Montes AD, Clavijo EG, Pascual FJR, Andonaegui P, Jeffries TE, Alcock JE, Fernández RD, Carmona AL (2009) A rootless suture and the loss of the roots of a mountain chain: the Variscan belt of NW Iberia. CR Geosci 341:114–126. https://doi.org/10.1016/j.crte.2008.11.004

Mazur S, Aleksandrowski P (2001) The Tepla(?)/Saxothuringian suture in the Karkonosze-Izera massif, western Sudetes, central European Variscides. Int J Earth Sci 90:341–360

Mazur S, Aleksandrowski P, Kryza R, Oberc-Dziedzic T (2006) The Variscan Orogen in Poland. Geol Q 50:89–118

Mazur S, Kröner A, Szczepański J, Turniak K, Hanžl P, Melichar R, Rodionov NV, Paderin I, Sergeev SA (2010) Single zircon U/Pb ages and geochemistry of granitoid gneisses from SW Poland: evidence for an Avalonian affinity of the Brunian microcontinent. Geol Mag. https://doi.org/10.1017/S001675680999080X

Mazur S, Szczepański J, Turniak K, McNaughton NJ (2012) Location of the Rheic suture in the eastern Bohemian Massif: evidence from detrital zircon data. Terra Nova 24:199–206. https://doi.org/10.1111/j.1365-3121.2011.01053.x

Mazur S, Turniak K, Szczepański J, McNaughton NJ (2015) Vestiges of Saxothuringian crust in the Central Sudetes, Bohemian Massif: Zircon evidence of a recycled subducted slab provenance. Gondwana Res 27:825–839. https://doi.org/10.1016/j.gr.2013.11.005

McLennan SM (1989) Rare earth elements in sedimentary rocks; influence of provenance and sedimentary processes. Rev Mineral Geochem 21:169–200

McLennan SM, Hemming S, McDaniel DK, Hanson GN (1993) Geochemical approaches to sedimentation, provenance, and tectonics. Spec Paper Geol Soc Am 284:21–40

Meinhold G, Morton AC, Fanning CM, Frei D, Howard JP, Phillips RJ, Strogen D, Whitham AG (2011) Evidence from detrital zircons for recycling of Mesoproterozoic and Neoproterozoic crust recorded in Paleozoic and Mesozoic sandstones of southern Libya. Earth Planet Sci Lett 312:164–175. https://doi.org/10.1016/j.epsl.2011.09.056

Mingram B, Kröner A, Hegner E, Krentz O (2004) Zircon ages, geochemistry, and Nd isotopic systematics of pre-Variscan orthogneisses from the Erzgebirge, Saxony (Germany), and geodynamic interpretation. Int J Earth Sci 93:706–727

Murphy JB, Nance RD (1989) Model for the evolution of the Avalonian-Cadomian belt. Geology 17:735. https://doi.org/10.1130/0091-7613(1989)017<0735:MFTEOT>2.3.CO;2

Murphy JB, Gutierrez-Alonso G, Nance RD, Fernandez-Suarez J, Keppie JD, Quesada C, Strachan RA, Dostal J (2006) Origin of the Rheic Ocean: rifting along a Neoproterozoic suture? Geology 34:325. https://doi.org/10.1130/G22068.1

Murphy JB, Gutierrez-Alonso G, Nance RD, Fernandez-Suarez J, Keppie JD, Quesada C, Dostal J, Braid JA (2009) Rheic Ocean mafic complexes: overview and synthesis. Geol Soc Lond Spec Publ 327:343–369. https://doi.org/10.1144/SP327.15

Nance RD, Murphy JB, Strachan RA et al (1991) Late Proterozoic tectonostratigraphic evolution of the Avalonian and Cadomian terranes. Precambr Res 53:41–78. https://doi.org/10.1016/0301-9268(91)90005-U

Nance RD, Murphy JB, Keppie JD (2002) A Cordilleran model for the evolution of Avalonia. Tectonophysics 352:11–31. https://doi.org/10.1016/S0040-1951(02)00187-7

Nance RD, Murphy JB, Strachan RA, Keppie JD, Gutierrez Alonso G, Fernandez Suarez J, Quesada C, Linnemann U, d'Lemos R, Pisarevsky SA (2008) Neoproterozoic-early Palaeozoic tectonostratigraphy and palaeogeography of the peri-Gondwanan terranes; Amazonian v. West African connections. Geol Soc Spec Publ 297:345–383

Nance RD, Gutiérrez-Alonso G, Keppie JD, Linnemann U, Murphy JB, Quesada C, Strachan RA, Woodcock NH (2010) Evolution of the Rheic Ocean. Gondwana Res 17:194–222. https://doi.org/10.1016/j.gr.2009.08.001

Oberc-Dziedzic T, Kryza R, Pin Ch, Mochnacka K, Larionov A (2009) The Orthogneiss and Schist Complex of the

Karkonosze-Izera Mas sif (Sudetes, SW Poland): U–Pb SHRIMP zircon ages, Nd-iso tope systematics and protoliths. Geol Sudetica 41:3–24

Oberc-Dziedzic T, Kryza R, Mochnacka K, Larionov A (2010) Ordovician passive continental margin magmatism in the Central-European Variscides: U–Pb zircon data from the SE part of the Karkonosze-Izera Massif, Sudetes, SW Poland. Int J Earth Sci 99:27–46. https://doi.org/10.1007/s00531-008-0382-4

Oliver G, Corfu F, Krogh T (1993) U–Pb ages from SW Poland - evidence for a Caledonian suture zone between Baltica and Gondwana. J Geol Soc Lond 150:355–369

Pankhurst RJ, Hervé F, Fanning CM, Calderón M, Niemeyer H, Griem-Klee S, Soto F (2016) The pre-Mesozoic rocks of northern Chile: U–Pb ages, and Hf and O isotopes. Earth Sci Rev 152:88–105. https://doi.org/10.1016/j.earscirev.2015.11.009

Pastor-Galán D, Gutiérrez-Alonso G, Fernández-Suárez J, Murphy JB, Nieto F (2013) Tectonic evolution of NW Iberia during the Paleozoic inferred from the geochemical record of detrital rocks in the Cantabrian Zone. Lithos 182–183:211–228. https://doi.org/10.1016/j.lithos.2013.09.007

Pereira MF, Chichorro M, Linnemann U, Eguiluz L, Silva JB (2006) Inherited arc signature in Ediacaran and Early Cambrian basins of the Ossa-Morena Zone (Iberian Massif, Portugal); paleogeographic link with European and North African Cadomian correlatives. Precambr Res 144:297–315

Pereira MF, Linnemann U, Hofmann M, Chichorro M, Solá AR, Medina J, Silva JB (2012) The provenance of Late Ediacaran and Early Ordovician siliciclastic rocks in the Southwest Central Iberian Zone: Constraints from detrital zircon data on northern Gondwana margin evolution during the late Neoproterozoic. Precambr Res 192–195:166–189. https://doi.org/10.1016/j.precamres.2011.10.019

Peucat JJ, Drareni A, Latouche L, Deloule E, Vidal P (2003) U–Pb zircon (TIMS and SIMS) and Sm–Nd whole-rock geochronology of the Gour Oumelalen granulitic basement, Hoggar massif, Tuareg shield, Algeria. J Afr Earth Sci 37:229–239. https://doi.org/10.1016/j.jafrearsci.2003.03.001

Pollock JC, Hibbard JP, van Staal CR (2012) A paleogeographical review of the peri-Gondwanan realm of the Appalachian orogen, This article is one of a series of papers published in this CJES Special Issue: In honour of Ward Neale on the theme of Appalachian and Grenvillian geology. Can J Earth Sci 49:259–288. https://doi.org/10.1139/e11-049

R Core Team (2012) R: a language and environment for statistical computing. R Foundation for Statistical Computing, Vienna

Roser BP, Korsch RJ (1986) Determination of tectonic setting of sandstone—mudstone suits using SiO_2 content and K2O/Na2O ratio. J Geol 94:635–650

Sláma J, Košler J, Condon DJ, Crowley JL, Gerdes A, Hanchar JM, Horstwood MSA, Morris GA, Nasdala L, Norberg N, Schaltegger U, Schoene B, Tubrett MN, Whitehouse MJ (2008) Plešovice zircon—a new natural reference material for U–Pb and Hf isotopic microanalysis. Chem Geol 249:1–35. https://doi.org/10.1016/j.chemgeo.2007.11.005

Strachan RA, Linnemann U, Jeffries T, Drost K, Ulrich J (2014) Armorican provenance for the mélange deposits below the Lizard ophiolite (Cornwall, UK): evidence for Devonian obduction of Cadomian and Lower Palaeozoic crust onto the southern margin of Avalonia. Int J Earth Sci (Geol Rundsch) 103:1359–1383. https://doi.org/10.1007/s00531-013-0961-x

Szczepański J (2010) Proweniencjai ewolucja tektonometamorficzna serii suprakrustalnejw krystaliniku Gór Bystrzyckich. Provenance and tectonometamorphic evolution of the supracrustal series from the Bystrzyckie Mts. Crystalline Massif. Szczepański, Jacek

Szczepański J, Ilnicki S (2014) From Cadomian arc to Ordovician passive margin: geochemical records preserved in metasedimentary successions of the Orlica-Śnieżnik Dome in SW Poland. Int J Earth Sci 103:627–647. https://doi.org/10.1007/s00531-013-0993-2

Taylor SR, McLennan SM (1985) The continental crust; its composition and evolution; an examination of the geochemical record preserved in sedimentary rocks. Blackwell, New York

Taylor SR, McLennan SM (1995) The geochemical evolution of the continental crust. Rev Geophys 33:241–265

Tichomirowa M, Berger H-J, Koch EA, Belyatski BV, Götze J, Kempe U, Nasdala L, Schaltegger U (2001) Zircon ages of high-grade gneisses in the Eastern Erzgebirge (Central European Variscides)—constraints on origin of the rocks and Precambrian to Ordovician magmatic events in the Variscan foldbelt. Lithos 56:303–332. https://doi.org/10.1016/S0024-4937(00)00066-9

Torsvik TH (2017) Earth history and palaeogeography: Trond H. Torsvik, University of Oslo, and L. Robin M. Cocks, The Natural History Museum, London.

Turniak K, Mazur S, Wysoczański R (2000) SHRIMP zircon geochronology and geochemistry of the Orlica-Śnieżnik gneisses (Variscan belt of Central Europe) and their tectonic implications. Geodin Acta 13:293–312

Valverde-Vaquero P, Dörr W, Belka Z, Franke W, Wiszniewska J, Schastok J (2000) U–Pb single-grain dating of detrital zircon in the Cambrian of central Poland: implications for Gondwana versus Baltica provenance studies. Earth Planet Sci Lett 184:225–240. https://doi.org/10.1016/S0012-821X(00)00312-5

van Staal CR, Sullivan RW, Whalen JB (1996) Provenance of tectonic history of the Gander Zone in the Caledonian/Appalachian Orogen: implications for the origin and assembly of Avalon. In: Avalonian and related peri-Gondwanan terranes of the Circum-North Atlantic. GSA special paper, vol 304. Geological Society of America, pp 347–367

Verma SP, Armstrong-Altrin JS (2013) New multi-dimensional diagrams for tectonic discrimination of siliciclastic sediments and their application to Precambrian basins. Chem Geol 355:117–133. https://doi.org/10.1016/j.chemgeo.2013.07.014

Vintaned JAG, Schmitz U, Linan E (2009) Upper Vendian-lowest Ordovician sequences of the western Gondwana margin, NE Spain. Geol Soc Lond Spec Publ 326:231–244. https://doi.org/10.1144/SP326.13

von Raumer J, Stampfli G, Borel G, Bussy F (2002) Organization of pre-Variscan basement areas at the north-Gondwanan margin. Int J Earth Sci 91:35–52. https://doi.org/10.1007/s005310100200

Wiedenbeck M, Allé P, Corfu F, Griffin WL, Meier M, Oberli F, Quadt AV, Roddick JC, Spiegel W (1995) Three natural zircon standards for U-TH-PB, LU-HF, trace element and Ree analyses. Geostand Geoanal Res 19:1–23. https://doi.org/10.1111/j.1751-908X.1995.tb00147.x

Willner AP, Gerdes A, Massonne H-J et al (2014) Crustal evolution of the northeast Laurentian margin and the Peri-Gondwanan microcontinent Ganderia prior to and during closure of the Iapetus ocean: detrital zircon U–Pb and Hf isotope evidence from Newfoundland. Geosci Canada 41:345. https://doi.org/10.12789/geocanj.2014.41.046

Žáčková E, Konopásek J, Košler J, Jeřábek P (2010) Detrital zircon populations in quartzites of the Krkonoše-Jizera Massif: implications for pre-collisional history of the Saxothuringian Domain in the Bohemian Massif. Geol Mag 149:443–458. https://doi.org/10.1017/S0016756811000744

Žák J, Sláma J (2018) How far did the Cadomian 'terranes' travel from Gondwana during early Palaeozoic? A critical reappraisal based on detrital zircon geochronology. Int Geol Rev 60:319–338. https://doi.org/10.1080/00206814.2017.1334599

Żelaźniewicz A, Dörr W, Bylina P, Franke W, Haack U, Heinisch H, Schastok J, Grandmontagne K, Kulicki C (2004) The eastern continuation of the Cadomian orogen: U–Pb zircon evidence from Saxo-Thuringian granitoids in south-western Poland and the northern Czech Republic. Int J Earth Sci 93:773–781. https://doi.org/10.1007/s00531-004-0418-3

Zieger J, Linnemann U, Hofmann M, Gärtner A, Marko L, Gerdes A (2017) A new U–Pb LA-ICP-MS age of the Rumburk granite (Lausitz Block, Saxo-Thuringian Zone): constraints for a magmatic event in the Upper Cambrian. Int J Earth Sci. https://doi.org/10.1007/s00531-017-1511-8